



UNIVERSITY OF LEEDS

This is a repository copy of *New constraints on micro-seismicity and stress state in the western part of the North Anatolian Fault Zone: Observations from a dense seismic array.*

White Rose Research Online URL for this paper:
<https://eprints.whiterose.ac.uk/87052/>

Version: Accepted Version

Article:

Altuncu-Poyraz, S, Teoman, U, Turkelli, N et al. (9 more authors) (2015) New constraints on micro-seismicity and stress state in the western part of the North Anatolian Fault Zone: Observations from a dense seismic array. *Tectonophysics*, 656. pp. 190-201. ISSN 0040-1951

<https://doi.org/10.1016/j.tecto.2015.06.022>

© 2015, Elsevier. Licensed under the Creative Commons Attribution-NonCommercial-NoDerivatives 4.0 International <http://creativecommons.org/licenses/by-nc-nd/4.0/>

Reuse

Items deposited in White Rose Research Online are protected by copyright, with all rights reserved unless indicated otherwise. They may be downloaded and/or printed for private study, or other acts as permitted by national copyright laws. The publisher or other rights holders may allow further reproduction and re-use of the full text version. This is indicated by the licence information on the White Rose Research Online record for the item.

Takedown

If you consider content in White Rose Research Online to be in breach of UK law, please notify us by emailing eprints@whiterose.ac.uk including the URL of the record and the reason for the withdrawal request.



eprints@whiterose.ac.uk
<https://eprints.whiterose.ac.uk/>

1 **New constraints on micro-seismicity and stress state in the western part of the North**
2 **Anatolian Fault Zone: Observations from a dense seismic array**

3

4 **Selda ALTUNCU POYRAZ¹, M. Uğur TEOMAN¹, Niyazi TÜRKELLİ¹, Metin**
5 **KAHRAMAN¹, Didem CAMBAZ¹, Ahu MUTLU¹, Sebastian ROST², Gregory A.**
6 **HOUSEMAN², David A. THOMPSON³, David CORNWELL³, Murat UTKUCU⁴**
7 **and Levent GÜLEN⁴**

8

9 ¹ B.U. Kandilli Observatory and Earthquake Research Institute, Department of Geophysics,
10 Istanbul, Turkey

11 Corresponding author. Tel: + 90 216 516 33 56; fax: + 90 216 516 38 06.

12 E-mail adres: selda.altuncu@boun.edu.tr

13

14 ²Leeds University, Institute of Geophysics and Tectonics, School of Earth and Environment,
15 Leeds, United Kingdom

16

17 ³ School of Geoscience, University of Aberdeen, King's College, Aberdeen, United Kingdom

18

19 ⁴Sakarya University, Geophysics Department, Sakarya

20

21 **Abstract**

22 With the aim of extensively investigating the crustal structure beneath the western segment of
23 the North Anatolian Fault Zone where it splays into northern and southern branches, a

24 temporary seismic network (Dense array for North Anatolia-DANA) consisting of 70 stations
25 was deployed in early May 2012 and operated for 18 months in the Sakarya region during the
26 FaultLab experiment. Out of 2437 events contaminated by explosions, we extracted 1371 well
27 located earthquakes. The enhanced station coverage having a nominal station spacing of 7
28 km, lead to a minimum magnitude calculation of 0.1. Horizontal and vertical location
29 uncertainties within the array do not exceed 0.8 km and 0.9 km, respectively. We observe
30 considerable seismic activity along both branches of the fault where the depth of the
31 seismogenic zone was mostly confined to 15 km. Using our current earthquake catalogue we
32 obtained a b -value of 1. We also mapped the b -value variation with depth and observed a
33 gradual decrease. Furthermore, we determined the source parameters of 41 earthquakes with
34 magnitudes greater than 1.8 using P-wave first motion polarity method. Regional Moment
35 Tensor Inversion method was also applied to earthquakes with magnitudes greater than 3.0.
36 Focal mechanism solutions confirm that Sakarya and its vicinity is stressed by a
37 compressional regime showing a primarily oblique-slip motion character. Stress tensor
38 analysis indicates that the maximum principal stress is aligned in WNW-ESE direction and
39 the tensional axis is aligned in NNE-SSW direction.

40

41 **1. Introduction**

42 The North Anatolian Fault Zone (NAFZ) is a large-scale continental strike slip fault
43 system extending from Karliova Junction in the east towards the Aegean domain in the west
44 cutting across the entire Northern Turkey (**Figure 1a**). This major plate boundary
45 accommodates most of the westward movement of the Anatolian Block. Recent GPS
46 measurements revealed a maximum slip rate of approximately 24 ± 1 mm/yr for the NAFZ and
47 a counterclockwise rotation of the Anatolian Block (Reilinger *et al.*, 1997; 2000; McClusky *et*
48 *al.*, 2000). The NAFZ displays a more or less linear character along most of its 1500 km

49 length until it splays into two main strands east of the Almacık Mountains (**Figure 1b**). The
50 northern strand dissects the Adapazari basin and traverses the Marmara Sea reaching the Gulf
51 of Saros (Şengör, 2005). The southern strand mostly remains on land and is not as well
52 developed considering the shallower depth of associated basins (Duman et al, 2005). It
53 extends through Pamukova and Iznik Lake and enters the Sea of Marmara at the Gulf of
54 Gemlik. Both the northern and southern strands bound two regions of uplift: the Almacık
55 Mountains and the Armutlu Peninsula.

56 The intense internal deformation has caused numerous destructive earthquakes along
57 the NAFZ throughout the 20th century. The most recent İzmit (17 August 1999, Mw:7.4) and
58 Düzce (12 November 1999, Mw:7.2) events are regarded as the western continuation of a
59 major earthquake sequence which started with the 1939 Erzincan earthquake in eastern
60 Turkey (Toksöz et al., 1979; Barka, 1996) rupturing a nearly 1000-km long segment of the
61 NAFZ. The proximity and rapid succession of these major events strongly implies an
62 interaction between sequence nucleation processes, yet the nature of this interaction is still
63 widely debated. Historical seismicity indicates that the İzmit earthquake occurred in an area
64 of Coulomb stress increase induced by major earthquakes and several authors have pointed
65 out the static triggering role of the İzmit event on the Düzce Earthquake (Parsons et al., 2000;
66 King et al., 2001; Utkucu et al., 2003). As shown in **Figure 1b**, the Izmit earthquake ruptured
67 the northern branch of the NAFZ along four distinct structural segments, namely the Golcuk,
68 Izmit-Sapanca, Sakarya and Karadere segments. Rupture lengths along each of these segment
69 varied between 25 km and 36 km with observed dextral displacements of 1.5-5m (Barka et. al,
70 2000). These segments are separated by right releasing stepovers wider than 1 km and/or gaps
71 in the fault trace (Langridge et al., 2002; Lettis et al., 2000). Further to the east, the Düzce
72 earthquake formed an east-west striking 40 km long rupture with an average lateral
73 displacement of 3.5 m, also including 9 km of rupture overlap with the eastern termination of

74 the İzmit rupture (Akyüz et al., 2002; Hartleb et al., 2002; Duman et al., 2005). The Düzce
75 rupture also consists of several segments separated by restraining stepovers. Both these
76 earthquakes were recorded extremely well by seismology and satellite geodesy (INSAR and
77 GPS), and the coseismic source models have been accurately determined (Wright et al., 2001;
78 Burgmann et al., 2002).

79 In the present study, we primarily focus on the western segment of the NAFZ (**Figure 1a**)
80 benefiting from a dataset collected from a dense seismic array (consisting of 70 temporary
81 broadband seismic stations and an additional 8 stations from the permanent network)
82 encompassing both the northern and southern strands of the fault covering part of the rupture
83 area of 1999 İzmit and Düzce earthquakes. This array was mainly designed to determine the
84 fine scale structure of the crust in this area and to image the structure of the NAFZ in the
85 lower crust. With the help of this new and extensive data set, our main objective is to provide
86 new insights on the most recent micro-seismic activity and the relevant b -value. Furthermore,
87 we used our focal mechanism solutions in order to put additional constrains on the current
88 stress orientation in this region.

89

90 **2. Data and Methods**

91 Within the framework of the FaultLab project which is funded by National Environment
92 Research Council (NERC-UK), the DANA array consisting of 70 broadband stations (54
93 CMG6TD, 6 CMG3TD, 2 CMGESPD and 1 CMG40TD sensors provided by the SEIS-UK
94 instrument pool) was deployed in the Sakarya-Adapazarı region and operated from early May
95 2012 to late September 2013. In order to further improve the station coverage, DANA
96 includes seven additional CMG6TD broadband sensors surrounding the array and installed by
97 KOERI/department of Geophysics with support from Boğaziçi University Research Fund.
98 Eight permanent stations of KOERI (CMG3TDs) were also included in our analysis. Data

99 were recorded at 50Hz sampling. The array was composed of six parallel lines forming a 2-D
100 grid crossing both the northern and southern branches of NAFZ, supplemented by a further 7
101 stations arranged in an arc on the east side (**Figure 2a**). The nominal station spacing of the
102 stations was 7 km, which was achieved for majority of the stations.

103

104 **2.1. Micro-seismicity and b-value Analysis**

105 Local events were visually identified and extracted from the continuous data. Event
106 locations were determined using HYPO71 (Lee and Lahr, 1972) implemented in ZSAC, an
107 interactive software package developed at KOERI (Yilmazer, 2012). A well constrained 1D
108 velocity model (modified from Karabulut et al., 2011) was used in the location algorithm
109 which is shown in Table 1. The station configuration of this experiment with dense station
110 spacing significantly enhanced the event detection capability and allowed us to locate a total
111 of 2437 seismic events with a minimum local magnitude (M_L) of 0.1 during the deployment
112 of DANA network. M_L magnitudes for epicentral distances less than 200 km were calculated
113 using the formula from Baumbach et al., (2003).

114 Due to the rapidly growing resource extraction industry, several active quarries and mining
115 areas exist in the study area. In order to properly constrain the earthquake related seismicity,
116 contaminations caused by any explosions and quarry blasts must be eliminated from the event
117 catalogue. We performed a statistical time of day analysis by searching daytime events versus
118 nighttime events and plotting them as a function of geographic location. Taking into account
119 the origin times of the events presented by the histogram in Figure 3a, we selected the
120 daytime interval between 08:00 and 16:00 separating the events into 8 hr day-night segments.
121 The logarithmic ratio of daytime to nighttime events is defined by the Q_m parameter (Wiemer
122 and Baer, 2000; Kekoali et al., 2011). The region was divided into different overlapping
123 square cells and we found that a cell size of 5 km x 5km contained sufficient number of

124 events to precisely identify the locations of quarry and mining areas. We limited our search to
125 crustal events with depths less than 20 km and magnitudes smaller than 3.0. The result of our
126 analysis shows that Q_m values vary from -0.57 to 4.17 (**Figure 3b**). We determined the blast
127 locations to have values of $Q_m \geq 2.5$. In order to test the accuracy of the analysis, we
128 compared these locations with current satellite images. In general, a good correlation was
129 observed suggesting that the daytime to nighttime ratio analysis can provide valuable
130 information on the location of potential quarry and mining areas. This analysis eliminated
131 mining related explosions from the catalog and we identified 1371 earthquakes (**Figure 2a**,
132 list also given as supplementary material S1) following the discrimination process. The vast
133 majority (~96%) of the earthquake depths are approximately confined to the upper 15 km of
134 the crust as shown in the depth histogram given in Figure 2b. Moreover, a magnitude
135 histogram in Figure 2c demonstrates the detection capability of DANA network. The majority
136 of the horizontal and vertical location uncertainties were found to be less than 0.8 km and 0.9
137 km, respectively. However, towards the edges of the array where the station coverage is less
138 dense, we observed relatively higher uncertainties (**Figure 4a**). The vast majority of the
139 average RMS arrival-time misfits were calculated within the range of 0.05-0.4 seconds as
140 indicated in **Figure 4b**. Figure 4c demonstrates the M_L standard deviations which do not
141 exceed 0.1 within the DANA array; however, towards the edges (42 events from cluster C in
142 Figure 2a) we calculated magnitude errors within the range of 0.3-0.4. Overall, azimuthal gap
143 values vary between 21° and 220° . Based on the travel time plots for 31595 Pg and 18416 Sg
144 phase readings given in **Figure 5a**, we calculated average seismic velocities of 5.95 km/sec
145 and 3.46 km/sec for Pg and Sg phases, respectively. We also extracted a V_p/V_s ratio of 1.713
146 from the Wadati diagram given in **Figure 5b** which is slightly lower than our starting value of
147 1.74.

148

149 We also performed a b -value analysis, a significant parameter to characterize seismicity in
150 a tectonically active region. Physically, the b -value describes the proportion of seismic energy
151 released by small versus large earthquakes; for a greater b -value the number of large
152 magnitude earthquakes is fewer relative to the number of small earthquakes. It can be
153 extracted from the slope of cumulative earthquake occurrence vs magnitude curve (**Figure 6**).
154 Moreover, the state of stress has a major effect in determining the character of the magnitude–
155 frequency distribution (Mori and Abercrombie, 1997; Toda et al., 1998). On average, b is
156 close to unity for most seismically active regions (e.g. Froelich & Davis 1993) but can vary
157 from 0.3-2.5 (El-Isa and Eaton, 2014). Low b -values are associated with major earthquakes
158 (Öncel et al., 1996) and asperities subjected to high stress (Wiemer & Wyss 1997), whereas
159 high values are related to decreased shear stress (Urbancic, 1992), extensional stress (Froelich
160 and Davis, 1993), etc. In the present study, b -values are calculated using a maximum
161 likelihood approach adopted in the ZMAP code (Utsu, 1999; Wiemer and Katsumata, 1999).
162 Using the 1371 earthquakes in our data set, we calculated a magnitude completeness (M_c)
163 value of 0.7 and a b -value of 1.0 ± 0.03 (**Figure 6b**). M_c calculation is based on the maximum
164 curvature method (Wiemer and Wyss, 2000). Both values are remarkably lower than the
165 comparable values for the KOERI catalogue spanning the same area and the operation period
166 of the DANA array (M_c : 1.7; b -value 1.32 ± 0.06 , **Figure 6a**).

167

168 **2.2. Fault Plane Solutions and Stress Tensor Inversion**

169 We applied the P-wave first arrival method from Suetsuge (1998) to obtain the fault
170 plane parameters for earthquakes with moment magnitude $M_L \geq 1.8$ (**Table 2**). Furthermore,
171 we also used the Regional Moment Tensor (RMT) inversion method of Dreger (2002) to infer
172 the source parameters of the earthquakes with magnitudes greater than 3.0. This method
173 adopts a least squares approach and makes use of full wave-form modeling which can provide

174 reliable constraints on the source orientation using data from sparsely distributed broadband
175 stations or even single broadband station (Dreger and Helmberger, 1993; Walter, 1993;
176 Dreger and Woods, 2002). The earthquake fault plane parameters (strike, dip, and rake) and
177 the seismic moment can be obtained directly from the moment tensor description. The
178 preparation of data involved a quality check of the three component waveforms. Stations with
179 recording gaps and signals with signal-to-noise ratio lower than 4.0 were eliminated.
180 Synthetic seismograms were computed using a frequency wavenumber algorithm (Saika,
181 1994). Green's functions were computed using crustal structure from Karabulut et al, (2011).
182 We obtained fault plane parameters of 41 earthquakes recorded within the operation period of
183 the seismic network (**Table 2**). Solutions from both methods are in good agreement
184 predominantly indicating right lateral strike-slip faulting along both branches of NAFZ with a
185 few exceptions in the vicinity of Akyazi region where we observed normal faulting (**Figure**
186 **7**). A comparison of both methods for the Serdivan mainshock is given as a supplementary
187 material (S4).

188 Fault plane solutions play a key role in determining the stress field orientation
189 (Gephart and Forsyth, 1984; Michael, 1984; Gephart and Forsyth, 1990; Bohnhoff et al.,
190 2004). We applied a stress analysis method developed by Gephart and Forsyth (1984) which
191 was implemented in a focal mechanism stress inversion code (FMSI; Gephart and Forsyth,
192 1990). Generally speaking, stress is defined by three principal axes (σ_1 , σ_2 , σ_3) using a tensor
193 description. The tectonic regime is directly related to the dip angles between these axes and
194 the horizontal plane. The stress amplitude ratio (R) defined by the equation $R = (\sigma_2 - \sigma_1) / (\sigma_3 - \sigma_1)$,
195 is used to assess the dominant stress state and explain the overall relation between the
196 principal axes. More detailed explanations on R are given by Bellier and Zoback (1995). The
197 method is based on the relation between the σ_1 , σ_2 , σ_3 components and the pressure (P)
198 tension (T) axes in accordance with the Anderson faulting theory (McKenzie 1970). FMSI

199 calculates the parameters σ_1 , σ_2 , σ_3 and R for each event in the cluster assuming that spatial
200 and temporal variations do not occur in the stationary stress field and slip occurs in the
201 direction of the maximum resolved shear stress on the fault plane. In order to accurately
202 constrain the stress field, we compiled the fault plane parameters obtained from the DANA
203 network and various other studies (Öcal, 1960; Canitez and Uçer, 1967; Nowroozi, 1972;
204 Canitez and Büyükaşikoğlu, 1983; Taymaz et al., 1991; Örgülü, 2001; Kalafat, 2009).

205 Figure **8A** illustrates the stress tensor inversion results from the focal mechanism solutions
206 of the 1999 İzmit earthquake and its aftershocks from previous studies (references in Table 2).
207 As seen in **Figure 8A**, the inversions calculated the best fitting stress tensor with azimuth and
208 plunge values of $\sigma_1=(110, 0)$, $\sigma_2=(201,58)$, $\sigma_3=(20, 32)$, and stress amplitude ratio $R=0.35$
209 indicating a transtensional regime similar to the regime found by Kiratzi (2002) and Pinar et
210 al., (2010). Inversions from the focal mechanisms obtained in this study resulted in a stress
211 tensor with azimuth and plunge values of $\sigma_1=(103, 27)$, $\sigma_2=(256,61)$, $\sigma_3=(7, 11)$, and stress
212 amplitude ratio $R=0.45$ as given in **Figure 8B**. The measure of the reliability of the solution is
213 the average misfit rotation angle calculated as 6.0° . This value reflects how well the individual
214 focal mechanisms fit the corresponding stress tensor. The greater the misfit angle, the less
215 spatially homogeneous is the stress field (Pinar et al., 2010; Hardebeck and Hauksson, 2001).

216

217 **3. Discussion and Conclusions**

218 The installation of a dense array across the NAFZ significantly enhanced the event
219 detection capability enabling us to accurately locate 1371 earthquakes (**Figure 2a**) within the
220 18 months recording period which is a strong evidence of high seismic activity.
221 Contaminations in the catalogue caused by blasts and mining activities were eliminated after
222 careful inspection. The seismogenic zone in the region surrounding the NAFZ is

223 approximately confined to the upper 15 km of the crust. During this seismic experiment we
224 recorded a moderate size earthquake (M_L :4.1) close to the town of Serdivan on 7 July 2012
225 (**Figure 2a**). We recorded 29 aftershocks within the following two-month period with
226 magnitudes varying from 0.4 to 2.2 (provided as supplementary material **S2 and S3**). The
227 aftershock distribution and focal mechanism solutions suggest that this activity might indicate
228 an unmapped continuation of a NE-SW oriented secondary fault located to the north of the
229 İzmit-Sapanca segment of NAFZ (**Figures 2, 6**). Based on our observations, a foreshock
230 activity has started nearly a month before the Serdivan mainshock, including a magnitude 2.3
231 earthquake which occurred approximately seven minutes prior to this earthquake (Provided as
232 supplementary material **S3**).

233 The recorded seismicity pattern displays several distinctive features. Although the
234 northern branch of NAFZ produces higher seismicity, we also located a considerable number
235 of earthquakes along the southern branch, namely the Geyve Fault. In addition to the
236 concentration of seismic activity along the north and south strands of the NAF, much
237 seismicity is located further north and south of the major fault strands. We observe a strong,
238 diffuse cluster of seismicity south of the Geyve fault (marked by a red ellipse B in Figure 2).
239 The occurrence of a nearby moderate size earthquake following the DANA array pull-out
240 (22.10.2014, M_L :4.5, black star in **Figure 2a** is a further indication of the continuous seismic
241 activity there. Further to the south of the Geyve fault, we observed a relatively diffuse cluster
242 close to city of Bilecik (marked by a red ellipse C in Figure 2a) indicating fault zone related
243 deformation away from the main fault. Two earthquake clusters were also mapped north of
244 Sakarya, in good agreement with the most recent active fault map published by Emre et al.,
245 (2013) from General Directorate of Mineral Research and Exploration (MTA). We located
246 another cluster in the vicinity of Akyazı at the junction of the Dokurcun fault, İzmit-Sakarya
247 and Duzce-Karadere fault segments (ellipse A in Figure 2a) forming a structural discontinuity

248 that contains several small scale faults, for which a higher rate of seismicity is expected. This
249 cluster occurs in a region of Coulomb stress increase, as reported by Utkucu et al., 2003.

250 The active fault map by MTA (Emre et al., 2013) indicates many relatively small scale
251 normal faults at the east of the Akyazı junction between the 1967 Mudurnu Valley and 1999
252 İzmit earthquake ruptures and the right stepping fault segments (**Figure 1b, and Figure 7**).
253 Barka et al., (2002) also measured a ~5m surface displacement following the 1999 İzmit
254 earthquake. Therefore relatively high b -values for the stepover area east of the junction should
255 be expected due to structural heterogeneity (King 1986; Wiemer and Katsumata, 1999; Liu et
256 al., 2003). The aftershock studies (Aktar, 2004; Özalaybey, 2002; Karabulut et al., 2002)
257 indicate a cluster of earthquakes in the fault junction, emphasizing a stress accumulation
258 following the İzmit earthquake. Calculation of the Coulomb stress change after the 1999
259 Düzce earthquake using all the large earthquakes also requires an increase in stresses for the
260 Akyazı junction. Interestingly, field studies indicated an about 10 km-long surface rupture gap
261 along the 1999 İzmit earthquake surface rupture in this region (Barka et al., 2002).. There had
262 been virtually no seismicity at the junction area before the 1999 İzmit earthquake (Gülen et
263 al., 2002), switching to a high aftershock activity (Özalaybey et al., 2002., Pınar et al., 2010)
264 following the earthquake. Our seismicity observations revealed that relatively high seismicity
265 rates persist at the junction and may still be associated with aftershock activity of the 1999
266 İzmit rupture. Long lasting aftershock activity is not unusual and is supported by global
267 observations (Stein and Liu, 2009; Parsons, 2009). It seems that both the redistribution of
268 stresses following the mainshock and the static stresses imparted by the large earthquake
269 rupture along the fault segments results in stress enhancement at the junction and the
270 generation of long-lasting seismic activity.

271 As shown in Figure 6, we calculated a b -value of 1 for the DANA array. This result is in
272 good agreement with the values revealed in a national report by Earthquake Engineering

273 Department of KOERI (Erdik et al., 2006). Figure 9 demonstrates the depth variation of the b -
274 value extracted from our final earthquake catalogue (excluding the events with magnitude
275 errors higher than 0.2). **Figure 9** also shows a gradual decrease in b -values with depth
276 beneath the fault. Similar observations have also been reported for the San Andreas Fault in
277 California (Mori and Abercrombie 1997; Wiemer and Wyss, 1997). The b -values tend to rise
278 in the shallow crust possibly due to presence of weak sedimentary layers and lower confining
279 pressure.

280 We determined the fault plane solutions of 41 earthquakes recorded within the array
281 using RMT and P-wave first motion polarity methods (**Table 2**). Solutions reveal right lateral
282 strike-slip faulting along both branches of NAFZ (**Figure 7**) with a few exceptions in the
283 vicinity of Akyazı region where we observed normal faulting possibly due to the existence of
284 stepovers (**Figure 1b**). RMT solutions for the 1999 Izmit and Düzce mainshocks show strike-
285 slip faulting and NE-SW extension that is well correlated with the tectonic regime and the
286 orientation of NAFZ (**Table 2**). Moreover, fault plane solutions of the M_L :4.1 Serdivan
287 mainshock, its aftershocks and foreshocks demonstrate two distinct fault planes. The first one
288 is NE-SW oriented dextral strike slip fault and the second one is NW-SE oriented sinistral
289 strike slip fault. The active fault map of MTA (Emre et al., 2013) shows a NE-SW striking
290 secondary fault in the vicinity of Serdivan seismic activity. Based on our findings, we
291 therefore suggest that the main fault plane is aligned in NE-SW direction with dextral strike
292 slip motion and the aftershock distribution marks the continuation of this fault.

293 Our stress tensor inversion results imply that maximum principal stress axes (σ_1) are
294 roughly WNW-ESE oriented and the horizontal minimum compressive stress axis (σ_3) is
295 NNE-SSW oriented (Figure 8B). The R -value calculated from the aftershock study of the
296 1999 İzmit earthquake (references in Table 2) varies within the 0-0.5 range and peaks at about
297 0.3 (Figure 8A). On the other hand, the R -value for the DANA survey peaks at a value closer

298 to 0.5, emphasizing that strike-slip is the dominant type of faulting. These results indicate
299 that the western part of the NAFZ is predominantly influenced by WNW compression and
300 NNE extension of similar magnitudes.

301 The deployment of a dense array in the area of a complicated continental strike-slip fault
302 allowed extremely low detection thresholds for micro-seismicity in the vicinity of recent
303 major earthquakes. The detected seismicity allows further insight into the deformation of the
304 Sakarya region and has highlighted several areas of previously unmapped active deformation.

305

306 **Acknowledgements**

307 Major funding was provided by the UK Natural Environment Research Council (NERC)
308 under grant NE/I028017/1 and partially supported by Boğaziçi University Research Fund
309 (BAP) under grant 6922. We would like to thank all the project members from the University
310 of Leeds, Boğaziçi University, Kandilli Observatory, Aberdeen University and Sakarya
311 University. I would also like to thank Prof. Ali Pinar and Dr. Kıvanç Kekovalıfor their
312 valuable comments. Some of the figures were generated by GMT software (Wessel and Smith
313 ,1995).

314

315

316

317

318

319

320

321 **References**

322

323 Aktar, M., Ozalaybey, S., Ergin, M., Karabulut, H., Bouin, M.-P., Tapırdamaz C., Biçmen, F.,
324 Yörük, A., Bouchon, M., 2004. Spatial variation of aftershock activity across the rupture
325 zone of the 17 August 1999 Izmit earthquake, Turkey. *Tectonophysics*, 391: 325-334.

326

327 Akyuz, H.S., Hartleb, R., Barka, A., Altunel, E., Sunal, G., Meyer, B., Armijo, R., 2002.
328 Surface Rupture and Slip Distribution of the 12 November 1999 Duzce Earthquake (M 7.1),
329 North Anatolian Fault, Bolu, Turkey. *Bulletin of the Seismological Society of America*, 92
330 (1): 61–66.

331

332 Barka, A., 1996. Slip distribution along the North Anatolian fault associated with large
333 earthquakes of the period of the period 1939-1967. *Bull. Seism. Soc. Am.*, 59:521–589.

334

335 Barka, A., S. Akyuz, E. Altunel, G. Sunal, Z. Cakir, A. Dikbas, B. Yerli, T. Rockwell, J.
336 Dolan, and R. Hartleb 2000. The August 17, 1999 Izmit earthquake, M 7.4, Eastern Marmara
337 region, Turkey: study of surface rupture and slip distribution, in *The 1999 Izmit and Duzce*
338 *Earthquakes: Preliminary Results*. Istanbul Technical University:349 pp.

339

340 Barka, A., H. S. Akyuz, E. Altunel, G. Sunal, Z. Cakır, A. Dikbas, B. Yerli, R. Armijo, B.
341 Meyer, J. B. de Chabalier, T. Rockwell, J. R. Dolan, R. Hartleb, T. Dawson, S.
342 Christofferson, A. Tucker, T. Fumal, R. Langridge, H. Stenner, W. Lettis, J. Bachhuber, and
343 W. Page, 2002. The surface rupture and slip distribution of the 17 August 1999 Izmit
344 earthquake (M 7.4), North Anatolian Fault. *Bull. Seismol. Soc. Am.*, 92: 43–60.

345

346 Bellier, O. and Zoback, M.,1995. Recent state of stress change in the Walker Lane zone
347 western basin and Range Province-USA. *Tectonics*, 14: 564– 593.

348

349 Baumbach, M., Bindi, D., Grosser, H., Milkereit, C., Parolai, S., Wang, R., Karakısa, S.,
350 Zümbül, S., Zschau, J., 2003. Calibration of an ML Scale in Northwestern Turkey from 1999
351 Izmit Aftershocks. *Bulletin of the Seismological Society of America*, Vol. 93, No. 5, pp.
352 2289–2295.

353

354 Bohnhoff, M., Baisch, S., Harjes, H.-P., 2004. Fault mechanisms of induced seismicity at the
355 superdeep German Continental Deep Drilling Program (KTB) borehole and their relation to
356 fault structure and stress field. *J. Geophys. Res.* 109, B02309. doi:10.1029/2003JB002528.

357

358 Canitez, N. and Üçer, S.B., 1967. Computer determinations for the fault plane solutions in
359 And Near Anatolia. *Tectonophysics*, 4(3):235-244.

360

361 Bürgmann, R., Ayhan, M.A., Fielding, E.J., Wright, Y., McClusky,S., Aktug, B., Demir, C.,
362 Lenk, O., Urkezer, A., 2002. Deformation during the 12 November 1999, Düzce, Turkey
363 Earthquake, from GPS and InSAR Data. *Bull. Seismol. Soc. Am.*, 92:161-171.

364

365 Canitez, N. and Büyükaşıkoglu, S., 1984. Seismicity of the Sinop Nuclear Power Plant Site,
366 Final Report, ITU, İstanbul.

367

368 Dreger, D.S. and Helmberger, D.V. , 1993. Determination of source at regional distances
369 With single stations or sparse network data. *J. Geophys. Res.* 98: 8107-8125.

370

371 Dreger, D.S. (2002), Time-Domain Moment Tensor Inverse Code (TDMT_INV) Release
372 1.1, (on internet www.seismo.berkeley.edu/~dreger).

373

374 Dreger, D. and Woods, B., 2002. Regional distance seismic moment tensors Of Nuclear
375 explosions. *Tectonophysics*, 356:139-156.

376

377 Duman, T. Y., Emre, Ö., Doğan, A., Özalp, S., 2005. Step-Over and Bend Structures along
378 the 1999 Duzce Earthquake Surface Rupture, North Anatolian Fault, Turkey. *Bulletin of the*
379 *Seismological Society of America*, Vol. 95, No. 4:1250–1262, doi: 10.1785/0120040082.

380

381 El-Isa, Z.H., and Eaton, D.W, 2014. Spatiotemporal variations in the *b*-value of earthquakes
382 magnitude-frequency distributions: Classifications and causes. *Tectonophysics*, Vol. 615-616:
383 1-11.

384

385 Emre, Ö., Duman, T. Y., Özalp, S., Elmacı, H., Olgun, Ş., Şaroğlu, F., 2013. Active fault map
386 of Turkey with an explanatory text 1:1,25,000. General Directorate of Mineral Research and
387 Exploration, Special Publication Series,30.

388

389 Erdik, M., Şeşetyan, K., Demircioğlu, M.B., Durukal, E., 2006. Ulaştırma Bakanlığı
390 Demiryolları, Limanlar ve Havameydanları İnşaatı Genel Müdürlüğü Kıyı Yapıları,
391 Demiryolları ve Havameydanları İnşaatları Deprem Teknik Yönetmeliği için Deprem
392 Tehlikesi Belirlenmesi, Report, Boğaziçi University, Kandilli Observatory and Earthquake
393 Research Institute, Department of Earthquake Engineering (In Turkish).

394

395

396 Froelich, H. C., and Davis, S., 1993. Teleseismic b values: or, much ado about 1.0. J.
397 Geophys. Res., 98: 631-644.

398

399 Gephart, J.W., Forsyth, D. W., 1984. An Improved method for determining the regional stress
400 tensor using earthquake focal mechanism data: Application to the San Fernando Earthquake
401 Sequence. Journal of Geophysical Research, 89:9305-9320.

402

403 Gephart, J.W., Forsyth, D. W., 1990. FMSI: A FORTRAN Program for Inverting
404 Fault/Slickenside and Earthquake focal mechanism data to obtain the regional stress tensor.
405 Computer&Geoscience, 16: 953-989.

406

407 Gülen, L., Pinar, A., Kalafat, D., Özel, N., Horasan, G., Yilmazer, M., Işıkara, A.M.,
408 2002. Surface fault breaks, aftershocks distribution, and rupture process of the 17 August 1999
409 Izmit, Turkey, earthquake. Bulletin of the Seismological Society of America 92:230–244.

410

411 Hardebeck, J. L., Hauksson, E., 2001. Stress Orientations Obtained from Earthquake Focal
412 Mechanisms: What Are Appropriate Uncertainty Estimates?. Bulletin of the Seismological
413 Society of America, 91(2): 250–262.

414

415 Hartleb, Ross D., Dolan, James F., Akyuz, H. Serdar, Dawson, Timothy E., Tucker, Allan
416 Z., Yerli, B., Rockwell, Thomas K., Toraman, Erkan., Cakir, Z., Dikbaş, A., Altunel, E.,
417 2002. Surface Rupture and Slip Distribution along the Karadere Segment of the 17 August
418 1999 Izmit and the Western Section of the 12 November 1999 Düzce, Turkey. Earthquakes
419 Bulletin of the Seismological Society of America, 92 (1): 67–78.

420

- 421 Kalafat, D., Kekovalı, K., Guneş, Y., Yılmaz, M., Kara, M., Deniz, P., Berberoğlu, M.,
422 2009. Türkiye ve çevresi Faylanma-Kaynak Parametreleri (MT) Kataloğu (1938- 2008)): A
423 Catalogue of source parameters of moderate and strong earthquakes for Turkey and its
424 surrounding area (1938-2008). Boğazici University Publications, No=1026, 43s., Bebek-
425 İstanbul.
- 426
- 427 Karabulut, H., Bouin, M.-P., Bouchon, M., Dietrich, M., Cornou, C., Aktar, M., 2002. The
428 seismicity in the eastern Marmara Sea after the 17 August 1999 Izmit earthquake. Bull. seism.
429 Soc. Am., 92: 387–393.
- 430 Karabulut, H., Schmittbuhl, J., Özalaybey, S., Lengliné, O., Kömeç Mutlu, A., Durand, V.,
431 Bouchon, M., Daniel, G., Bouin, M, P., 2011. Evolution of the seismicity in the eastern
432 Marmara Sea a decade before and after the 17 August 1999 Izmit earthquake, Tectonophysics,
433 510,17-27.
- 434 Kekovalı, K., Kalafat, D., Kara, M., Deniz, P., 2011. The estimation capability of potential
435 mining and quarry areas from seismic catalog using statistical analysis, an application to
436 Turkey. International Journal of the Physical Science Vol.6 (15):3704-3714.
- 437
- 438 King, G. C. P., 1986. Speculations on the geometry of the initiation and termination processes
439 of earthquake rupture and its relation to morphology and geologic structure: Pure and Applied
440 Geophysics, v. 124: 567-585.
- 441
- 442 King, G.C.P., Hubert-Ferrari, A., Nalbant, S.S., Meyer, B., Armijo, R., Bowman, D.,2001.
443 Coulomb interactions and the 17 August 1999 _Izmit, Turkey earthquake. Earth Planet Sci
444 333:557–569.

- 445 Kiratzi, A. A., 2002. Stress tensor inversions along the westernmost North Anatolian Fault
446 Zone and its continuation into the North Aegean Sea. *Geophys. J. Int.*, 151: 360–376.
447
- 448 Langridge, R.M., H. D. Stenner, T. E. Fumal, S. A. Christofferson, T. K. Rockwell, R. D.
449 Hartleb, J. Bachhuber, and A. A. Barka, 2002. Geometry, Slip Distribution, and Kinematics of
450 Surface Rupture on the Sakarya Fault Segment during the 17 August 1999 Izmit, Turkey.
451 *Bulletin of the Seismological Society of America*, 92 (1):107–125.
452
- 453 Lee WHK, Lahr JC (1972) HYPO71: a computer program for determining hypocenter,
454 magnitude and first-motion pattern of local earthquakes. U.S. Geological survey open-file
455 report: 100.
456
- 457 Lettis, W., J. Bachhuber, A. Barka, R. Witter, and C. Brankman., 2000. Surface fault rupture
458 and segmentation during the Kocaeli Earthquake, in *The 1999 Izmit and Duzce Earthquakes:
459 Preliminary Results*, A. Barka, O. Kozaci, S. Akyuz, and E. Altunel (Editors), Istanbul
460 Technical University, Istanbul: 349.
461
- 462 Liu, J., Sieh, K., Hauksson, E., 2003. A Structural Interpretation of the Aftershock ‘Cloud’ of
463 the 1992 Mw 7.3 Landers Earthquake. *Bull. Seismol. Soc. America.*, (93)3:1333-1344.
464
- 465 Mckenzie, D.P., 1970. Plate tectonics of the Mediterranean region. *Nature*, 226,:239-243.
466
- 467 Mckenzie, D.P., 1972. Active Tectonics of the Mediterranean region. *Geophys. J. R. Astr.*
468 *Soc.*, 30: 109-185.
469

470 McClusky, S., Balassanian, S., Barka, A., Demir, C., Ergintav, S., Georgiev, I., Gurkan, O.,
471 Hamburger, M., Hurst, K., Kahle, H., Kastens, K., Kekelidze, G., King, R., Kotzev, V., Lenk,
472 O., Mahmoud, S., Mishin, A., Nadariya, M., Ouzounis, A., Paradissis, D., Peter, Y., Prilepin,
473 M., Reilinger, R., Sanli, I., Seeger, H., Tealeb, A., Toksöz, M.N., Veis, G., 2000. Global
474 positioning system constraints on plate kinematics and dynamics in the eastern Mediterranean
475 and Caucasus. *J. Geophys. Res.* 105: 5695–5719.

476

477 Michael, A.J., 1984. Determination of stress from slip data: faults and folds. *J. Geophys. Res.*
478 89 :517–526.

479

480 Mori, J., Abercrombie, R. E., 1997. Depth dependence of earthquake frequency-magnitude
481 distributions in California: Implications for rupture initiation. *Journal of Geophysical*
482 *Research*, 102 (15): 081-090.

483

484 Nowroozi, A.A. 1972. Focal Mechanism of Earthquakes in Persia, Turkey, west Pakistan and
485 Afghanistan and plate tectonics of the middle east. *Bull. Seismol. Soc. America.*, 62: 823-850.

486

487 Öcal, N., 1960. Determination of the Mechanism of some Anatolian Earthquakes, A
488 Symposium on eq. mechanism. Vol.24 (10): 365-370.

489

490 Öncel, A.O., Main, I.G., Alptekin, Ö ., Cowie, P., 1996. Temporal variations in the fractal
491 properties of seismicity in the North Anatolian Fault Zone between 31⁰N and 41⁰E. *Pure appl.*
492 *Geophys.*, 146: 147–159.

493

- 494 Örgülü, G., Aktar, M., 2001. Regional moment tensor inversion for strong aftershocks of the
495 August 17, 1999 Izmit earthquake (Mw=7.4). *Geophys. Res. Lett.* 28 (2): 371–374.
496
- 497 Özalaybey, S., Ergin, M., Aktar, M., Tapırdamaz, C., Biçmen, F., Yörük, A., 2002. The 1999
498 _Izmit earthquake sequence in Turkey: seismological and tectonic aspects. *Bull Seismol Soc*
499 *Am* 92(1):376–386. doi: 10.1785/0120000838.
500
- 501 Parsons, T. (2009), Lasting earthquake legacy. *Nature*, v. 462: 41-42.
502
- 503 Parsons, T., Toda, S., Stein, R.S., Barka, A., Dieterich, J.H., 2000. Heightened odds of large
504 earthquakes near Istanbul: an interaction-based probability calculation. *Science* 288:661–665.
505 doi:10.1126/science.288.5466.661.
506
- 507 Pinar, A., Ucer, S.B., Honkura, Y., Sezgin, N., Ito, A., Baris, Ş., Kalafat, D., Matsushima, M.
508 and S. Horiuchi, 2010. Spatial variation of stress field along the fault rupture zone of the 1999
509 Izmit Earthquake. *Earth Planets Space*, 61(3):237-256.
510
- 511 Reilinger, R. E., S. C. McClusky, and M. B. Oral, 1997. GPS measurements of present day
512 crustal movements in the Arabia-Africa-Eurasia plate collision zone. *J. Geophys. Res.* , 102:
513 9983 –9999.
514
- 515 Reilinger, R. E., S. Ergintav, R. Burgmann, S. McClusky, O. Lenk, A. Barka, O. Gurkan, L.
516 Hearn, K. L. Feigl, R. Cakmak, B. Aktug, H. Ozener, M. N. Toksoz, 2000. Coseismic and
517 Postseismic Fault Slip for the 17 August 1999, M=7.5, Izmit, Turkey Earthquake. *Science*,
518 289: 1519–1524.

519

520 Saikia, C. K., 1994. Modified frequency-wavenumber algorithm for regional seismograms
521 using Filon's quadrature; modeling of Lg waves in eastern North America. *Geophysical*
522 *Journal International*, 118: 142-158.

523 Suetsugu, D., 1998. *Practise On Source Mechanism*. IISSE Lecture Note. Tsukuba, Japan,
524 p.104.

525

526 Stein, S., Liu, M., 2009. Long aftershock sequences within continents and implications for
527 earthquake hazard assessment. *Nature (Letters)*, vol:462:87-89.

528

529 Şengör, A.M.C., Tüysüz, O., İmren, C., Sakıncı, M., Eyidoğan, H., Görür, N., Xavier Le
530 Pichon, and Claude R., 2005. The North Anatolian Fault : A New Look Annual Review of
531 *Earth and Planetary Sciences*, Vol. 33: 37-112 .

532

533 Taymaz, T., Jackson, J.A., Mckenzie, D., 1991. Active Tectonics of the North and central
534 Aegean Sea. *Geophys. J. Int.*, 106: 433-490.

535

536 Toda, S., Stein, R.S., Reasenber, P.A., Dieterich, J.H., 1998. Stress transferred by the Mw =
537 6.5 Kobe, Japan, shock: effect on aftershocks and future earthquake probabilities. *Journal of*
538 *Geophysical Research* 103: 24543–24565.

539

540 Toksöz, M. N., Shakal A.F., Micheal A.J., 1979. Space-time migration of earthquakes along
541 the North Anatolian Fault Zone and seismic gaps. *Pure Appl Geophys* 117:1258–1270.
542 doi:10.1007/BF00876218.

543

544 Urbancic, T.I., Trifu, C.I., Long, J.M. & Toung, R.P., 1992. Space-time correlations of b-
545 values with stress release. *Pure appl. Geophys.*, 139: 449–462.

546

547 Utkucu, M., Nalbant, S., McClusky, J., Steacy, S., Alptekin, Ö., 2003. Slip distribution and
548 stress changes associated with the 1999 November 12, Düzce (Turkey) earthquake (Mw =
549 7.1). *Geophys J Int.*, 153:229–241. doi:10.1046/j.1365-246X.2003.01904.x

550

551 Utsu, T., 1999. Representation and analysis of the earthquake size distribution: a historical
552 review and some new approaches. *Pure Appl Geophys.*, 155:509–535.

553

554 Walter, R. W., 1993. Source parameters of the June 29, 1992 Little Skull Mountain
555 earthquake from complete regional waveforms at single station. *Geophys. Res. Lett.*, 20: 403-
556 406.

557

558 Wessel, P., Smith, W.H.F., 1995. New version of the generic mapping tools (GMT). *EOS*
559 *Trans.* 76: 329.

560

561 Wiemer S, Baer M., 2000. Mapping and removing quarry blast events from seismicity
562 catalogs. *Bull. Seismol. Soc. Am.*, 90(2): 525-530.

563

564 Wiemer S, Wyss M., 1997. Mapping the frequency-magnitude distribution in asperities: an
565 improved technique to calculate recurrence times. *Journal of Geophysical Research*,
566 102:15115–15128. doi:10.1029/97JB00726.

567

568 Wiemer, S., Katsumata, K., 1999. Spatial variability of seismicity parameters in aftershock
569 zones. *Journal of Geophysical Research*, 104: 13135–13151.

570 Wiemer, S., Wyss, M., 2000. Minimum magnitude of complete reporting in earthquake
571 catalogs: examples from Alaska, the Western United States, and Japan, *Bull. Seism. Soc. Am.*
572 90, 859-869.

573 Wright, T., Parsons, B., Fielding, E., 2001. Measurement of interseismic strain accumulation
574 across the North Anatolian Fault by satellite radar interferometry. *Geophys. Res. Lett.*,
575 28:2117-2120.

576

577 Yılmaz M., 2012. zSacWin: A Rapid Earthquake Processing and Archiving
578 System, User Guide v1.0. December 2012. Supported by the Research Fund of
579 the Boğaziçi University Project Number 5725P.

580

581 **Figure Captions**

582 **Figure 1: a)** Topographic map of the North Anatolian Fault Zone (NAFZ) region. Study area
583 is marked by a red square. Abbreviations; AP: Armutlu Peninsula, GB: Gemlik Bay, KJ:
584 Karlıova Junction, SB:Saros Bay **b)** Locations of fault ruptures associated with major
585 earthquakes in the western segment of NAFZ (modified from Lettis et al., 2002).

586

587 **Figure 2: a)** Local seismicity from May 2012 to September 2013. Most recent fault
588 information is taken from Emre et al., 2013. Abbreviations; ÇMF: Çilimli Fault, DB: Düzce
589 Basin, DKF:Dokurcun Fault, DZF:Düzce Fault, GYF:Geyve Fault, KDF: Karadere Fault.
590 Black star denotes one moderate size earthquake (ML: 4.5) recorded following the removal of
591 the DANA array. Bottom and right inserts show projections of earthquake depths onto North-

592 South and East-West profiles, respectively. Dashed red ellipses labelled *A*, *B*, *C* enclose
 593 regions of concentrated seismicity described further in the text. **b)** Earthquake depth
 594 histogram **c)** Earthquake magnitude histogram. We were able to precisely locate earthquakes
 595 with M_L magnitudes of 0.1.

596

597 **Figure 3: a)** Event-time histogram. **b)** Map showing the Q_m values for the study area. Darker
 598 green and blue colors ($Q_m > 2.5$) indicate the presence of possible blast locations.

599

600 **Figure 4: a)** Histogram of horizontal and vertical location uncertainties. **b)** Histogram of
 601 RMS arrival- time misfits. **c)** Histogram of M_L standard deviation.

602

603 **Figure 5: a)** Travel times for Pg and Sg Phases. The best linear fit to the travel time data are
 604 shown by the red lines. **b)** Wadati diagram obtained using higher quality picks. Red line
 605 indicates the best linear fit corresponding to a V_p/V_s value of 1.713.

606

607 **Figure 6:** Comparison of cumulative number of earthquakes, M_c and the b -value found **a)**
 608 using the KOERI catalogue and **b)** using the DANA dataset. The Serdivan mainshock
 609 ($M_L:4.1$) is indicated by the yellow star. The existence of such a dense seismic network
 610 significantly decreased the M_c threshold and has permitted to a more accurate determination
 611 of the b -value.

612

613 **Figure 7:** Focal mechanism solutions. Red beachballs show the 41 solutions from the current
 614 study and black beachballs indicate the solutions from various earlier studies listed in Table 2.
 615 Number 34 indicates the $M_L: 4.1$ Serdivan mainshock.

616

617 **Figure 8:** Stress tensor analysis from the P and T axes of the focal mechanisms. **A)** Analysis
 618 result for the 1999 İzmit Earthquake and its aftershocks, **B)** Analysis result for the $M \geq 1.8$
 619 earthquakes occurring within the operation period of DANA. Both panels show (a) the
 620 histogram of the R-value, (b) the distribution of the estimated principal stress axes and (c) the
 621 distribution of the observed P and T axes. In **(b)**, red solid dots show the azimuth and plunge
 622 of the maximum compression axis σ_1 , blue circles denote the minimum stress axis σ_3 and
 623 green triangles indicate the intermediate stress axis σ_2 . In **(c)**, red solid dots and blue circles
 624 show the P-axes and the T-axes, respectively. Black symbols denote the axes for the best
 625 fitting stress model.

626

627 **Figure 9:** **a)** b -value variation with depth. Horizontal bars reflect the uncertainty in b - value
 628 estimations while vertical bars indicate the depth range sampled for the assigned window of
 629 300 earthquakes. **b)** The selected area including the corresponding earthquakes. The colors
 630 indicate different depth (z) ranges.

631

632 **Table Captions**

633 **Table 1:** 1-D velocity model modified from Karabulut et al., (2011).

634

635 **Table 2:** The locations and source parameters of earthquakes ($M \geq 1.8$) in Sakarya region and
 636 surroundings compiled from our work and the previous studies. (1-McKenzie (1972), 2-
 637 Canitez and Büyükaşikoğlu (1984), 3-Canitez and Uçer (1967), 4-Öcal (1960), 5- Nowroozi
 638 (1972), 6- Taymaz et al (1991), 7- Örgülü (2001), 8- Kalafat et al (2009), HRV- Harvard
 639 Centroid-Moment Tensor Project.

Table1[Click here to download Table: Table1.docx](#)

Depth (km)	V_p (km/s)
0	3.27
2	5.75
4	5.85
6	5.90
8	5.91
12	6.15
16	6.50
20	6.84
24	6.84
28	6.84
30	6.84
32	7.34
36	7.89
40	7.89

Table2

[Click here to download Table: Table2.docx](#)

no	Date (d.m.y)	Time-GMT (h.m.s)	Latitude (N)	Longitude (E)	M_L	M_w	h(km)	Plane 1			Reference
								Strike	Dip	Rake	
1	20.06.1943	15:32:54	40.85	30.51	6.2	6.4	10	176	76	2	1,2
2	20.02.1956	20:31:43	39.89	30.49	6.0	6.2	40	264	50	-133	1,3
3	26.05.1957	06:33:35	40.67	31.00	6.6	6.7	10	87	78	176	1,2,3,4
4	22.07.1967	16:56:58	40.67	30.69	6.3	6.2	33	93	90	176	1,5,6
5	22.07.1967	17:48:06	40.66	30.62	4.9	5.2	26	110	72	-17	8
6	17.08.1999	03:14:01	40.60	30.63	5.5	5.3	8	192	34	-82	7
7	17.08.1999	05:10:08	40.72	30.01	4.6	4.7	6	29	80	-173	7
8	17.08.1999	05:45:23	40.74	30.01	4.7	4.3	11	243	45	-163	7
9	17.08.1999	06:01:32	40.75	29.99	4.0	4.1	4	263	69	147	7
10	17.08.1999	00:01:37	40.75	29.86	--	7.6	17	91	87	164	HRV,USGS
11	18.08.1999	01:04:25	40.66	30.77	4.0	4.0	6	182	39	-77	7
12	19.08.1999	13:04:13	40.64	30.58	4.0	4.5	9	195	53	-83	7
13	20.08.1999	15:59:02	40.78	30.93	4.1	4.1	10	246	57	150	7
14	22.08.1999	14:31:00	40.67	30.77	4.4	4.1	9	276	72	-165	7
15	31.08.1999	18:10:51	40.75	29.97	4.6	5.0	11	82	71	-133	7
16	31.08.1999	08:33:25	40.74	29.97	4.2	4.4	11	68	70	-142	7
17	04.09.1999	10:30:53	40.73	30.02	4.0	4.0	13	224	43	153	7
18	13.09.1999	11:55:28	40.31	30.29	--	5.8	15	176	86	-31	HRV
19	17.09.1999	19:50:07	40.75	30.08	4.5	4.4	18	170	82	-21	7
20	07.11.1999	16:54:42	40.57	31.36	--	5.0	15	269	71	106	HRV
21	11.11.1999	14:41:25	40.95	30.10	--	5.7	15	208	86	-41	HRV
22	12.11.1999	16:57:20	40.76	31.16	--	7.2	10	170	80	-36	HRV,USGS
23	23.08.2000	13:41:27	40.68	30.72	--	5.3	15	152	74	-34	HRV
24	17.09.2002	12:05:00	40.81	30.58	--	3.7	6	237	59	-95	8
25	01.04.2003	07:51:00	40.73	30.68	--	3.9	8	21	78	-19	8
26	22.06.2011	14:00:52	40.5623	31.1257	3.0		5.0	325	87	-72	FaultLab
27	11.07.2011	16:09:11	40.1562	29.9545	4.6		6.0	105	77	-66	FaultLab
28	24.02.2012	06:56:05	40.6382	30.5040	2.8		1.8	259	76	-168	FaultLab
29	11.06.2012	15:00:05	40.8982	30.4223	1.9		4.6	17	81	-178	FaultLab
30	12.06.2012	12:22:50	40.7682	30.4058	2.2		5.0	215	69	-175	FaultLab
31	22.06.2012	01:57:55	39.8902	30.6258	2.7		5.0	47	45	-43	FaultLab
32	28.06.2012	17:46:07	40.4862	30.1423	2.1		6.8	77	88	163	FaultLab
33	01.07.2012	06:06:30	40.7750	30.8367	2.2		7.5	56	58	158	FaultLab
34	07.07.2012	07:07:45	40.7643	30.3798	4.1	4.1	6.0	218	74	-178	FaultLab
35	07.07.2012	06:56:02	40.7632	30.3962	2.0		11.6	16	89	164	FaultLab
36	07.07.2012	07:14:25	40.7642	30.3925	2.2		11.6	203	86	172	FaultLab
37	07.07.2012	07:24:34	40.7635	30.3978	1.9		10.8	223	72	175	FaultLab
38	07.07.2012	09:20:12	40.7632	30.3918	1.9		9.8	208	83	-176	FaultLab
39	10.07.2012	09:13:42	40.4580	30.0448	2.6		9.4	236	83	-175	FaultLab

40	16.07.2012	07:41:59	40.7465	30.7723	2.2		9.0	59	89	158	FaultLab
41	17.08.2012	08:03:23	40.7623	30.3988	1.9		8.8	66	82	134	FaultLab
42	14.10.2012	08:36:39	40.7048	30.3037	2.6		11.6	143	54	154	FaultLab
43	24.10.2012	01:03:59	40.7027	30.6742	2.1		8.1	22	56	-162	FaultLab
44	02.11.2012	13:19:09	40.7672	30.3870	2.2		9.2	47	83	-163	FaultLab
45	09.11.2012	20:03:53	40.6978	30.6255	2.1		11.9	338	79	-69	FaultLab
46	13.11.2012	18:17:30	40.7173	30.1558	2.1		4.9	3	49	-8	FaultLab
47	16.11.2012	01:54:57	39.8087	30.5162	3.5		5.0	125	68	-66	FaultLab
48	09.12.2012	04:45:36	40.6930	30.6233	3.5	3.5	5.0	335	73	-64	FaultLab
49	09.12.2012	13:58:37	40.7105	30.6667	2.0		10.8	72	68	-143	FaultLab
50	18.01.2013	03:04:20	40.6977	30.6270	2.0		10.3	359	67	-5	FaultLab
51	23.01.2013	12:44:48	40.3977	30.1605	2.6		1.8	53	89	-172	FaultLab
52	14.02.2013	17:54:37	40.8797	30.6942	2.7		12	82	79	-147	FaultLab
53	24.02.2013	05:09:06	40.7563	30.2688	2.5		11.4	257	88	-174	FaultLab
54	26.02.2013	04:04:54	40.7533	30.2730	2.0		11.3	259	86	-172	FaultLab
55	07.03.2013	09:22:15	40.5693	30.5390	2.5		5.2	11	68	-151	FaultLab
56	13.04.2013	07:33:48	40.5198	30.4830	1.9		6.9	354	79	11	FaultLab
57	23.04.2013	15:19:56	40.7597	30.3650	3.2	3.1	2.0	41	74	-150	FaultLab
58	09.05.2013	03:52:56	40.5760	30.5427	2.3		3.1	30	84	-131	FaultLab
59	22.05.2013	22:38:47	40.6917	30.6463	2.0		9.8	105	53	-120	FaultLab
60	27.05.2013	06:38:30	40.6862	30.4180	1.9		6.9	341	59	-144	FaultLab
61	02.06.2013	22:58:03	40.7137	30.1447	2.0		5.0	11	72	-33	FaultLab
62	08.06.2013	12:08:55	40.6862	30.5387	2.3		11.9	36	71	-133	FaultLab
63	30.06.2013	02:53:56	40.6850	30.6542	1.8		14.6	254	88	133	FaultLab
64	30.06.2013	03:22:06	40.6882	30.6097	3.2		3.5	9	77	-59	FaultLab
65	02.07.2013	01:45:09	40.7897	30.7195	2.1		8.0	19	65	13	FaultLab
66	10.11.2013	02:09:24	40.7417	30.2575	3.5	3.4	9.6	265	87	-49	FaultLab

Figure1a-1b
[Click here to download high resolution image](#)

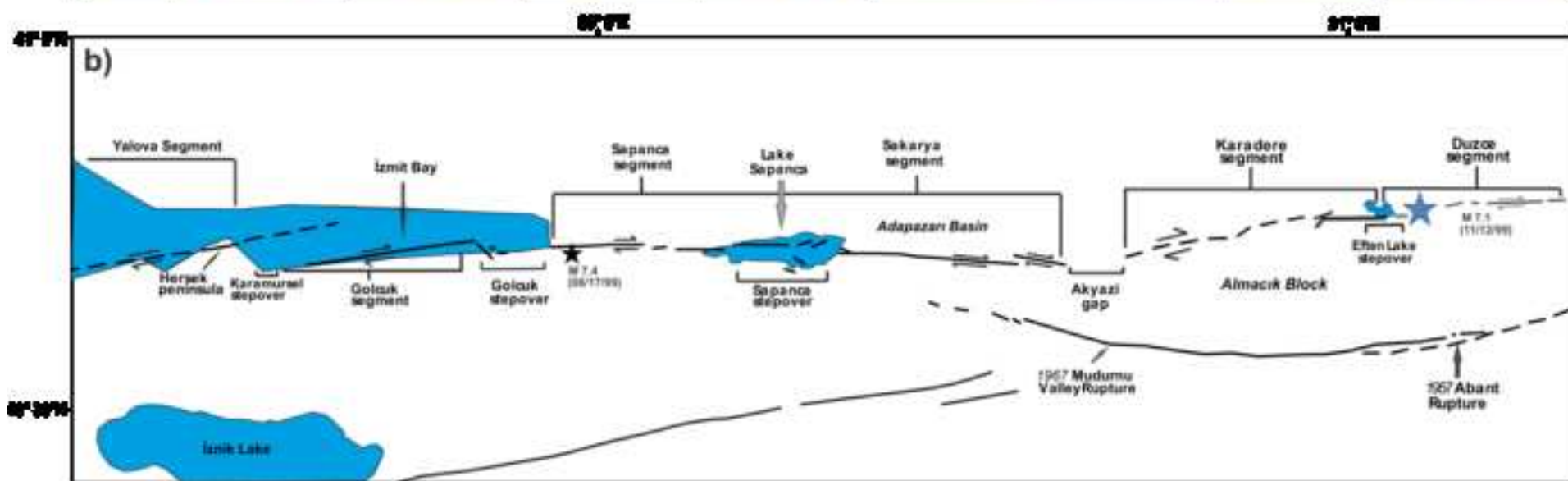
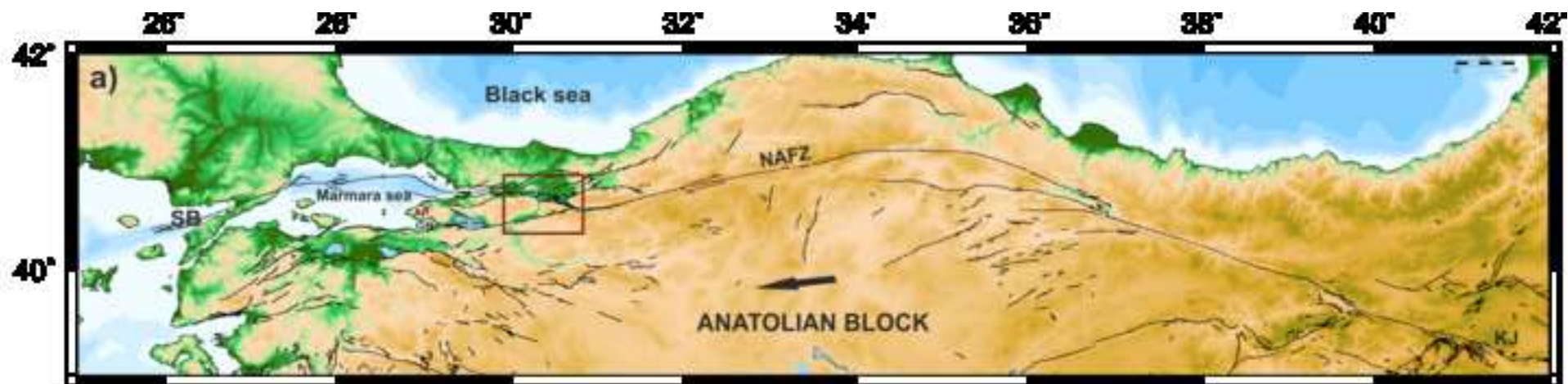


Figure 2a

[Click here to download high resolution image](#)

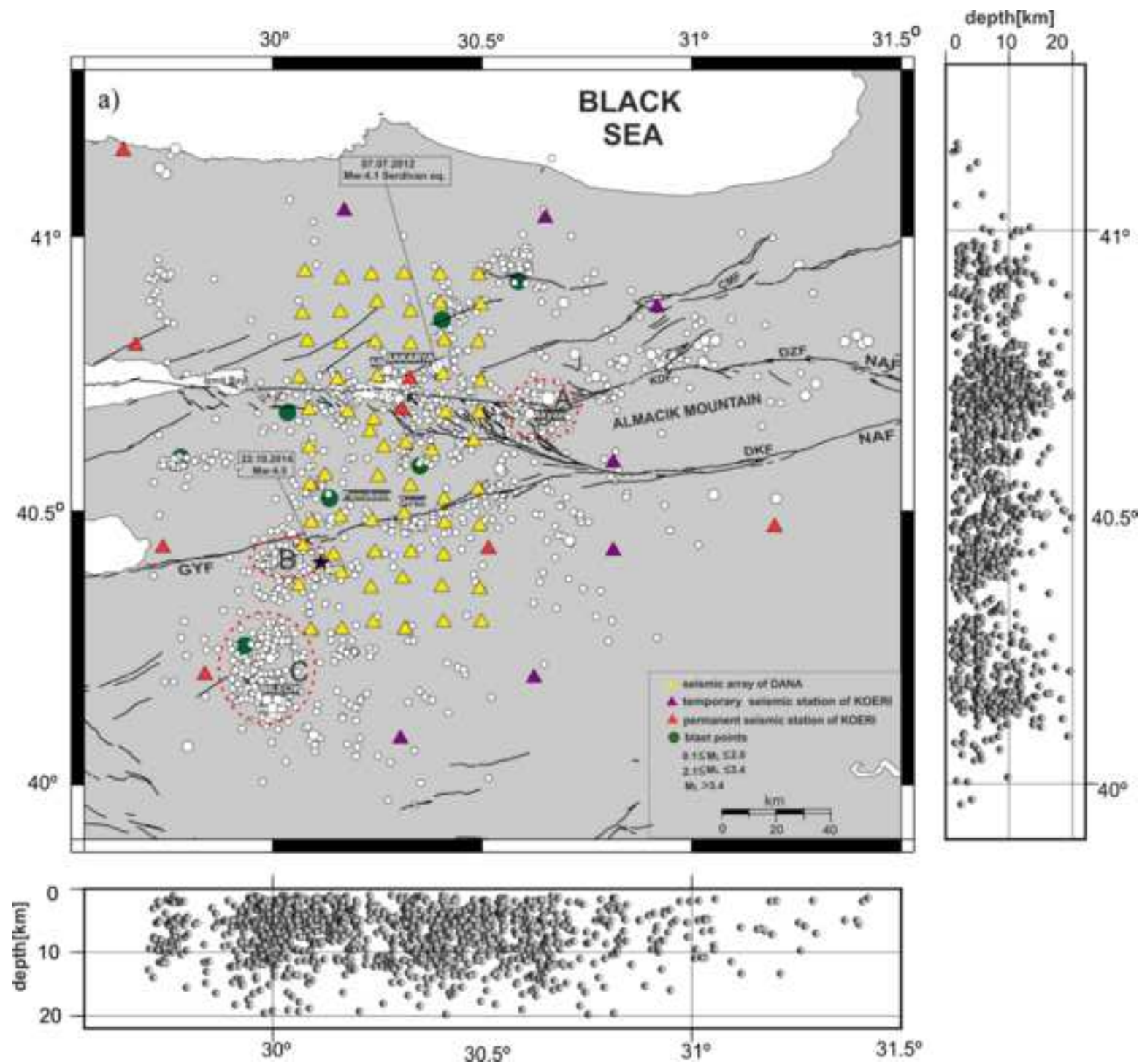


Figure 2b
[Click here to download high resolution image](#)

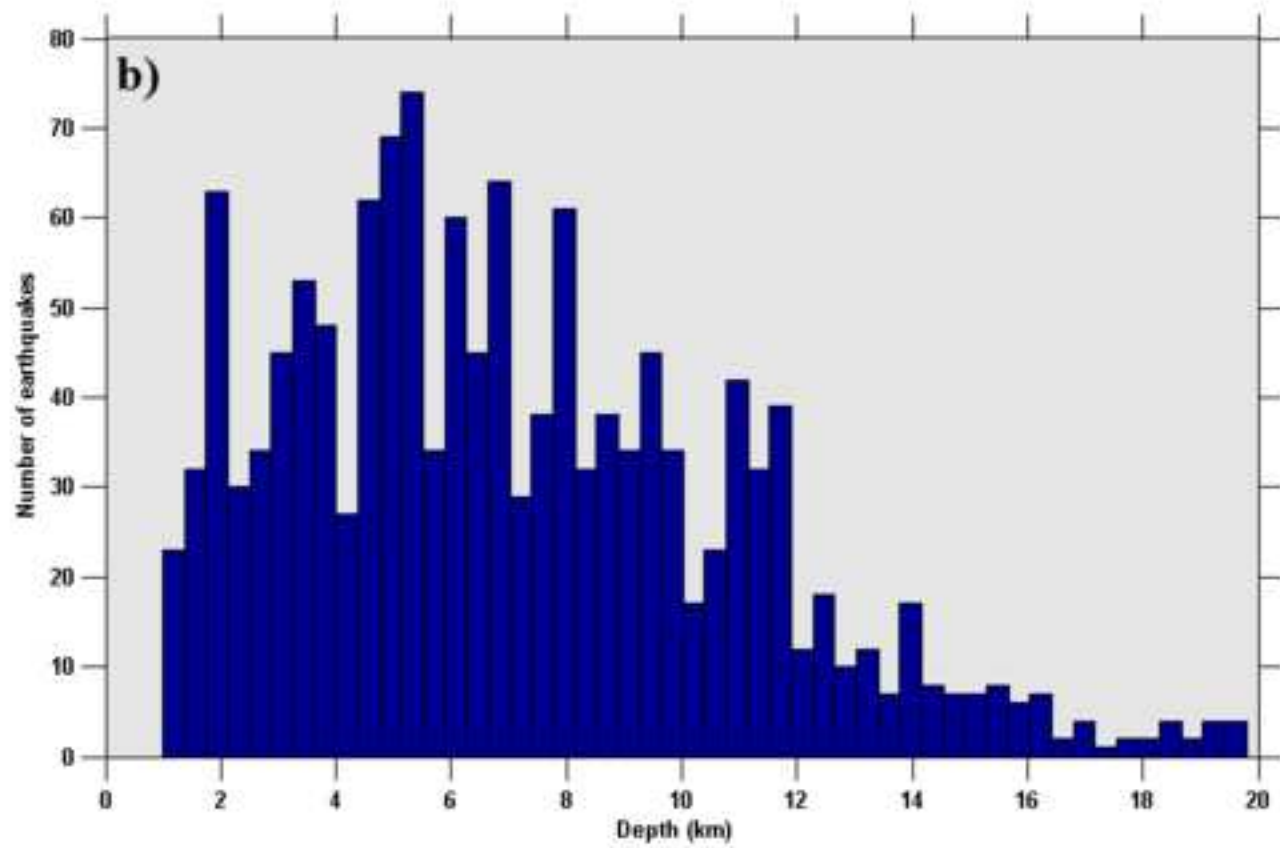


Figure 2c
[Click here to download high resolution image](#)

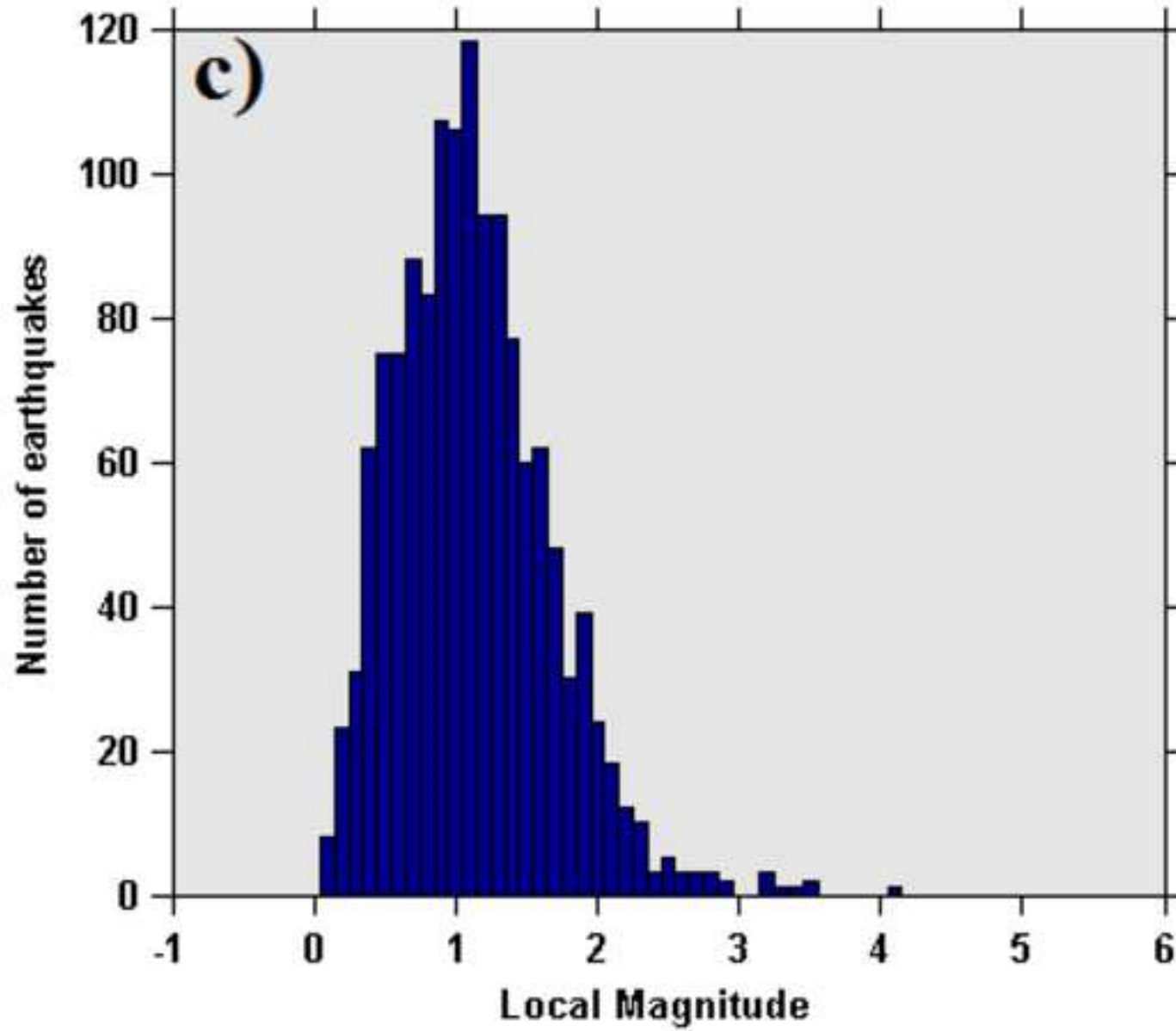


Figure 3a

[Click here to download high resolution image](#)

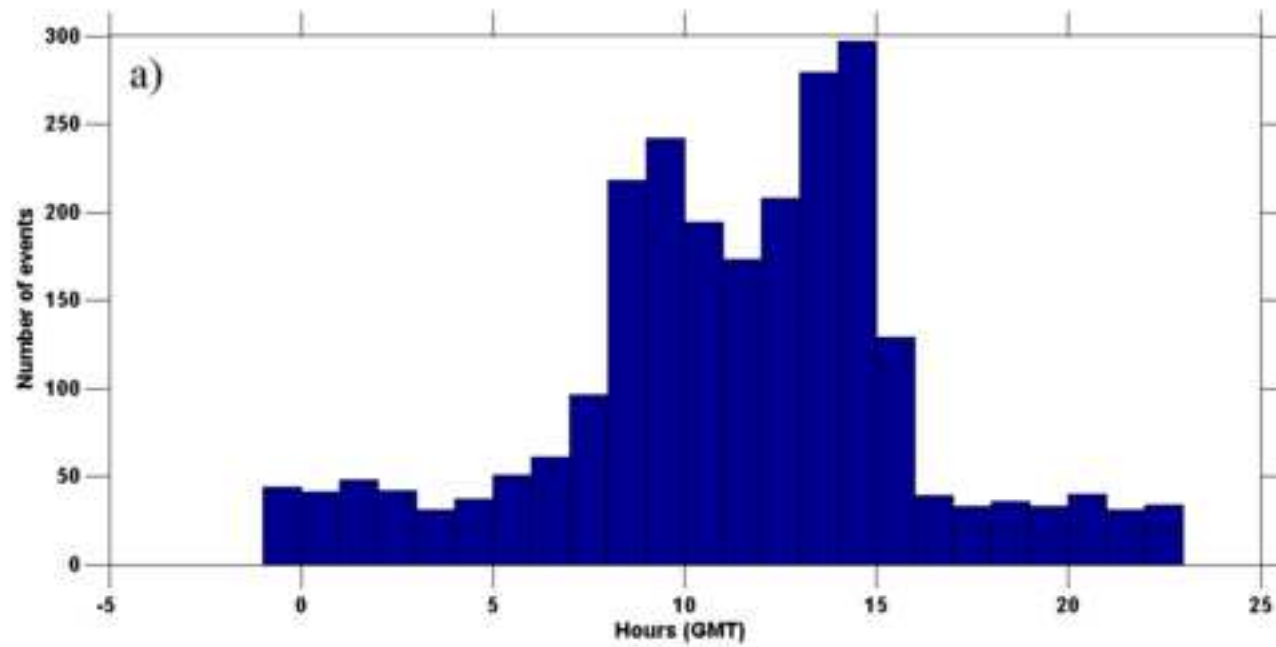


Figure 3b
[Click here to download high resolution image](#)

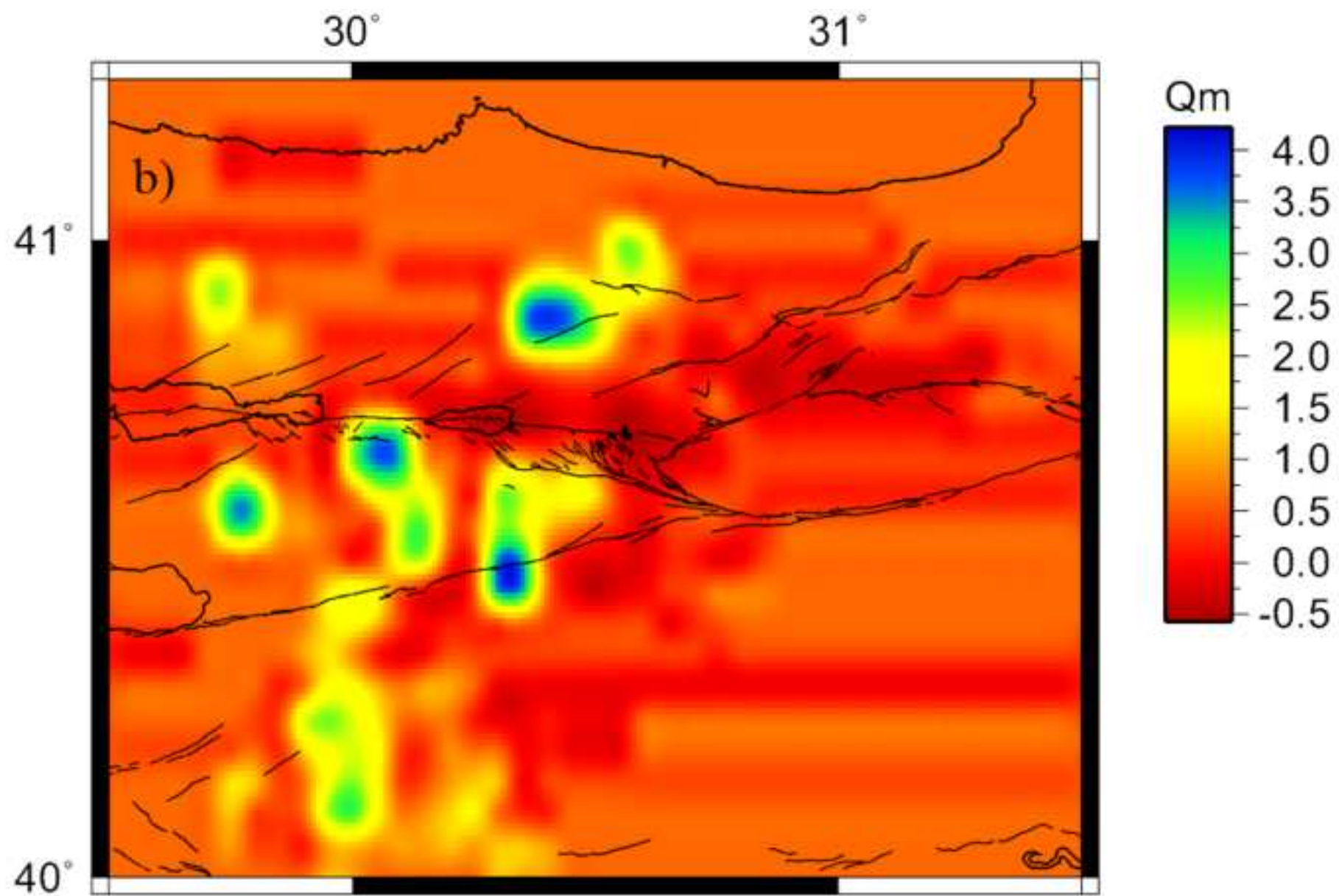


Figure 4a
[Click here to download high resolution image](#)

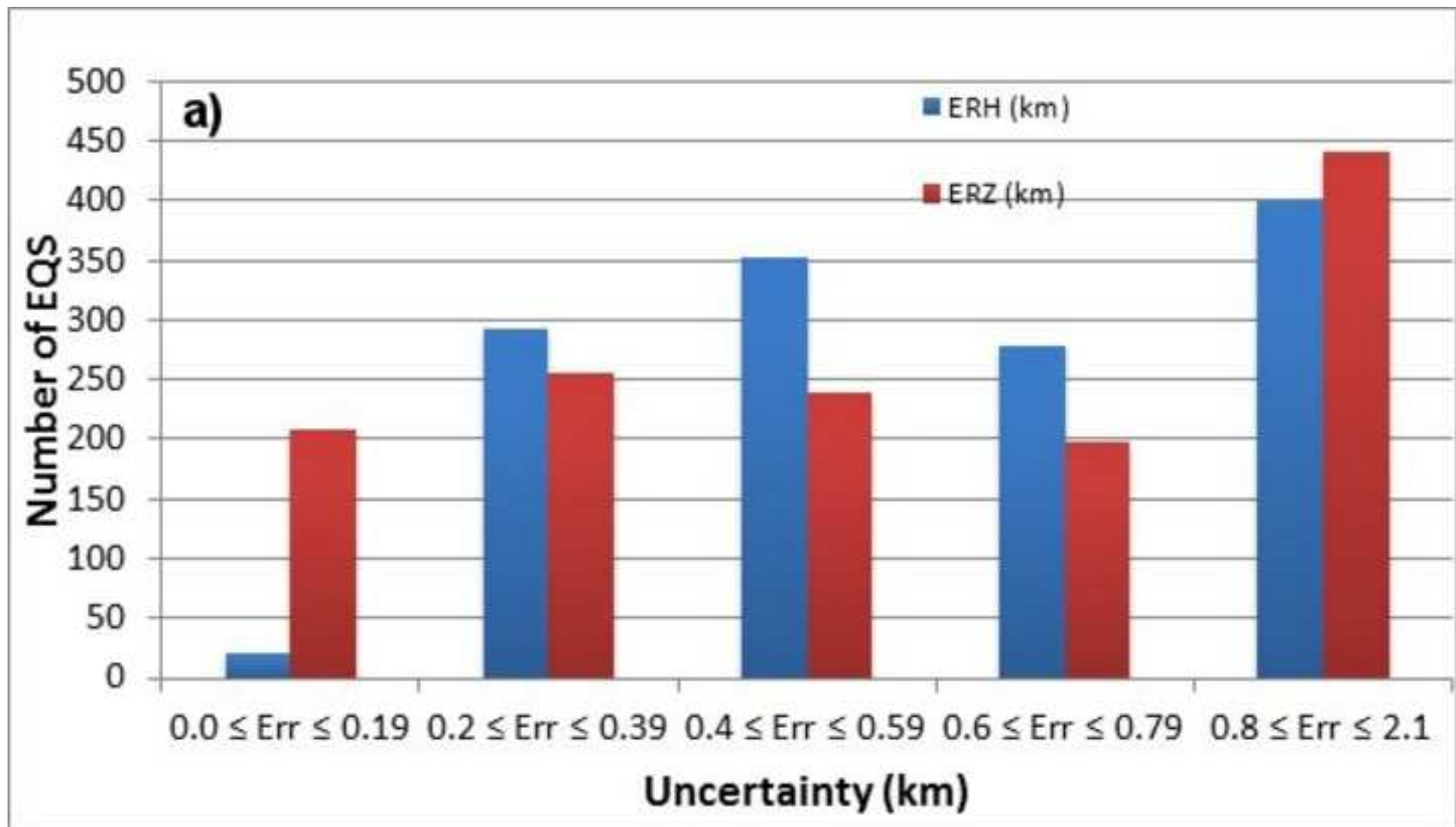


Figure 4b
[Click here to download high resolution image](#)

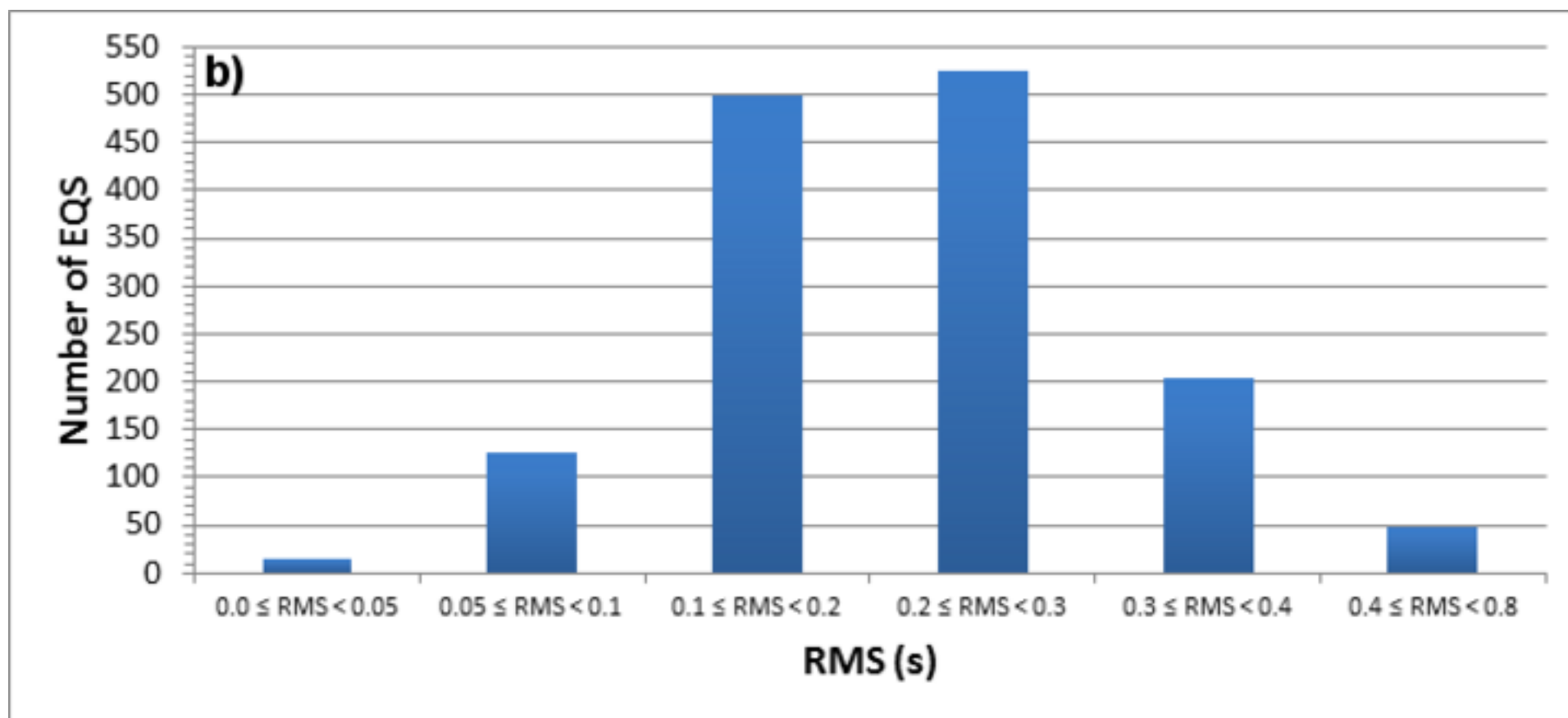


Figure 4c
[Click here to download high resolution image](#)

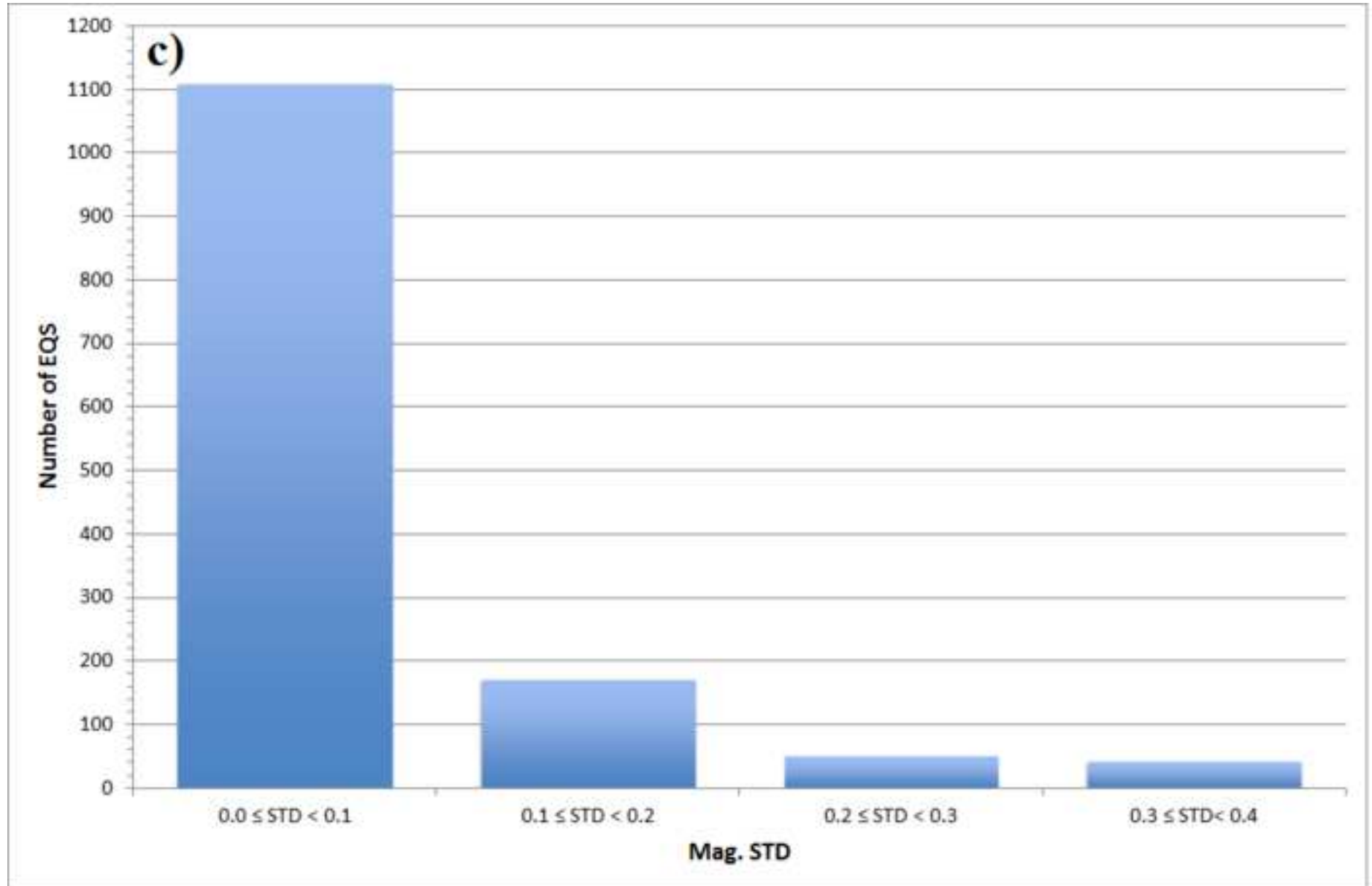


Figure 5a
[Click here to download high resolution image](#)

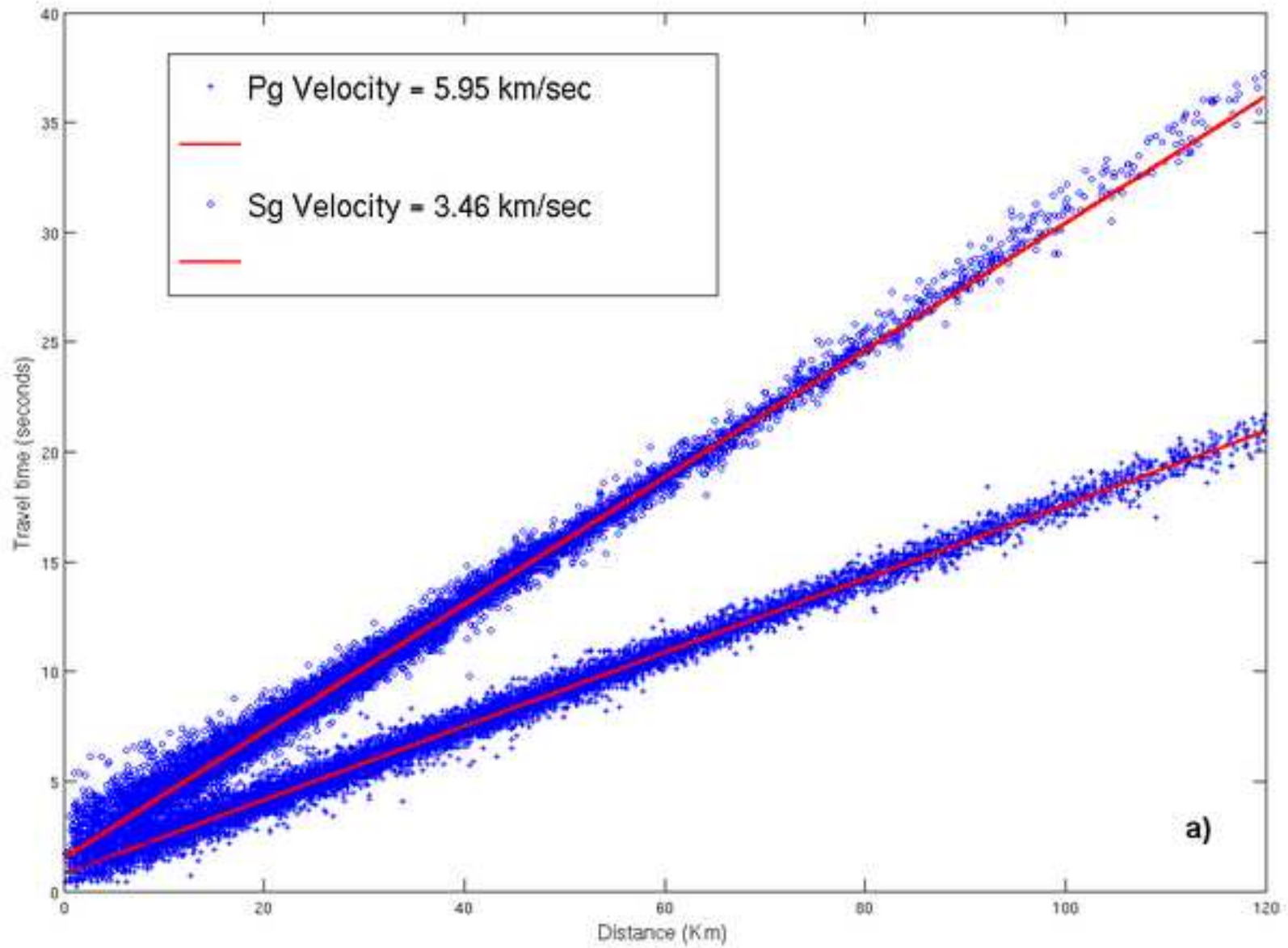


Figure 5b
[Click here to download high resolution image](#)

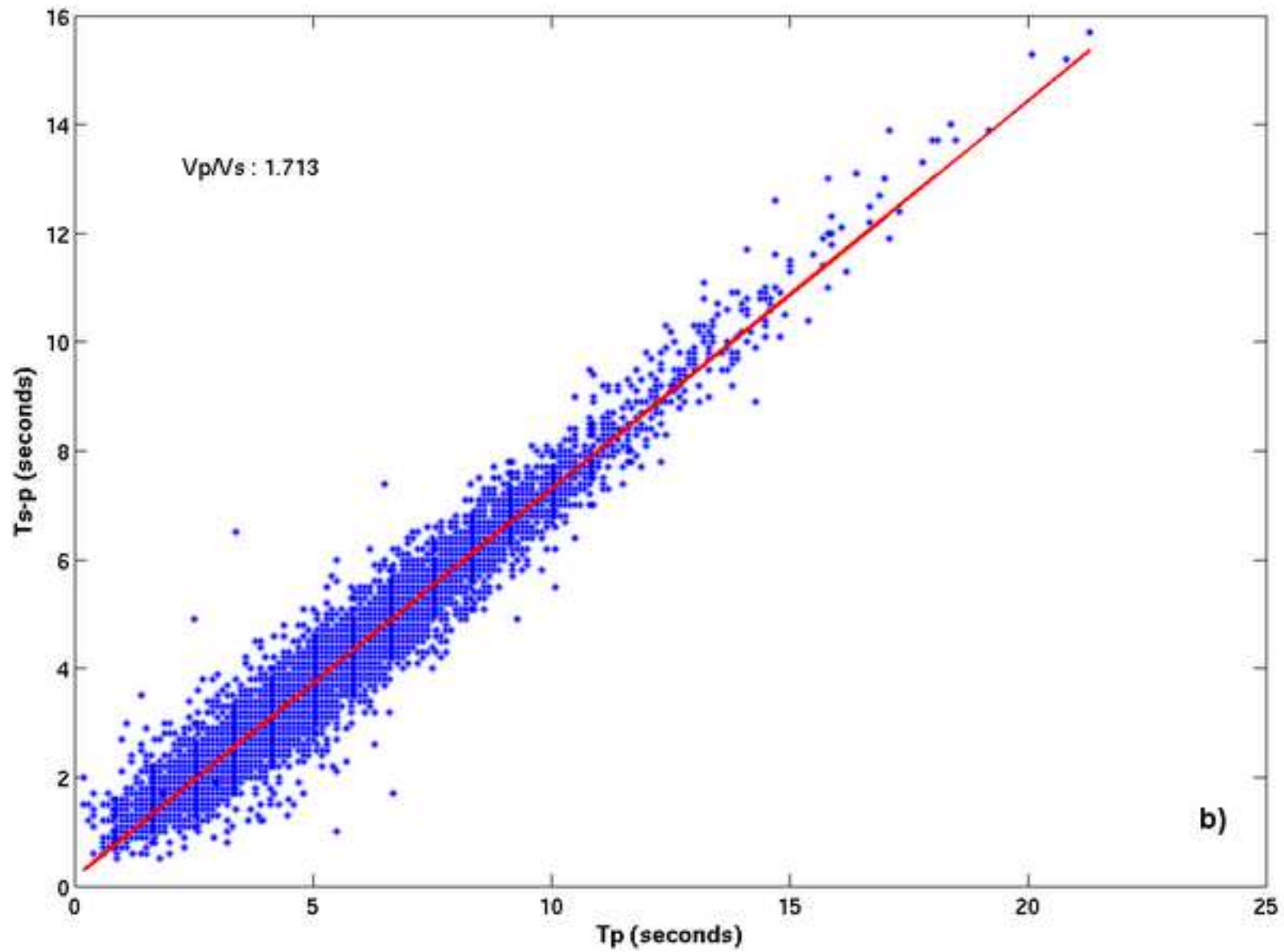


Figure 6

[Click here to download high resolution image](#)

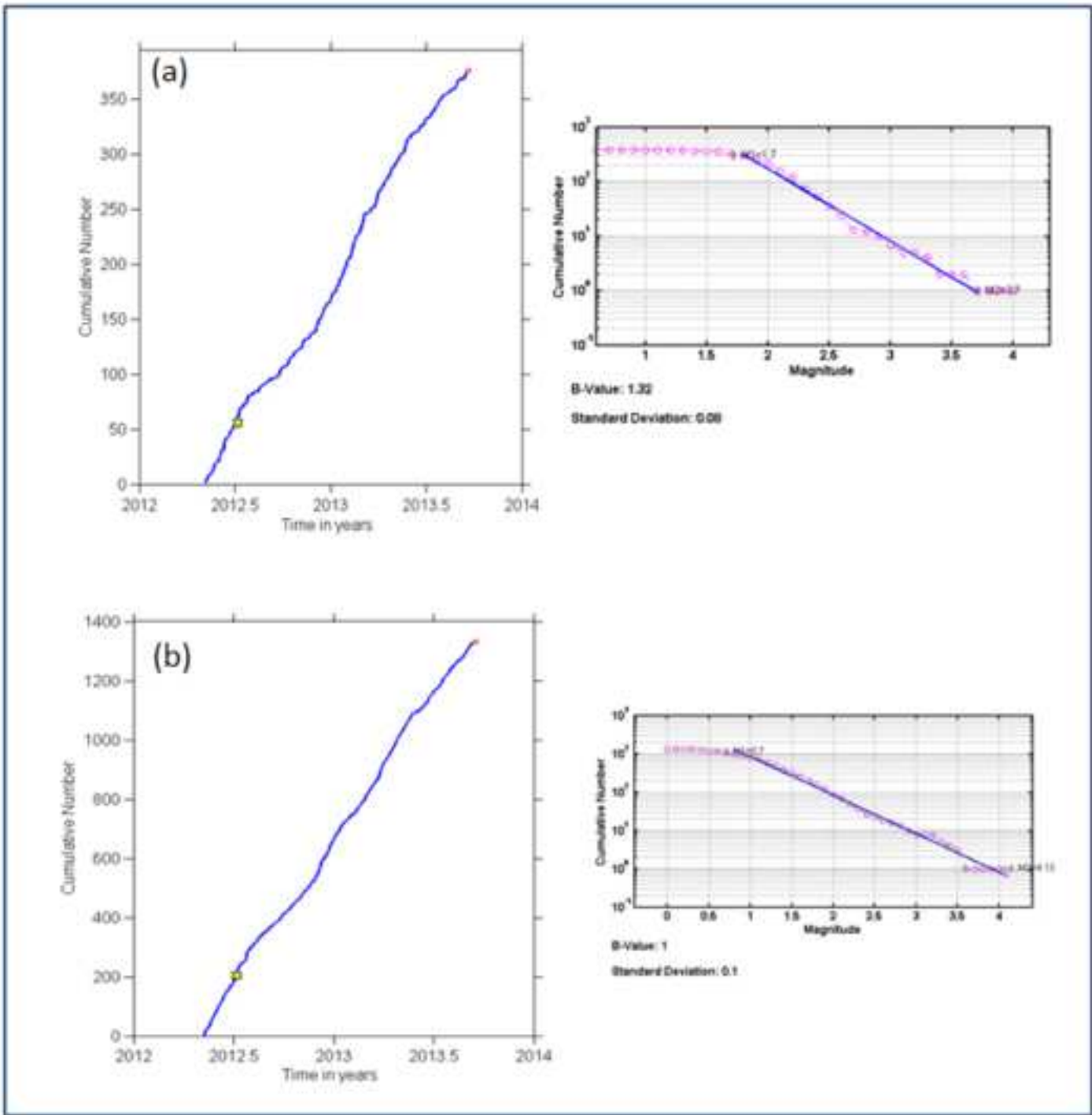
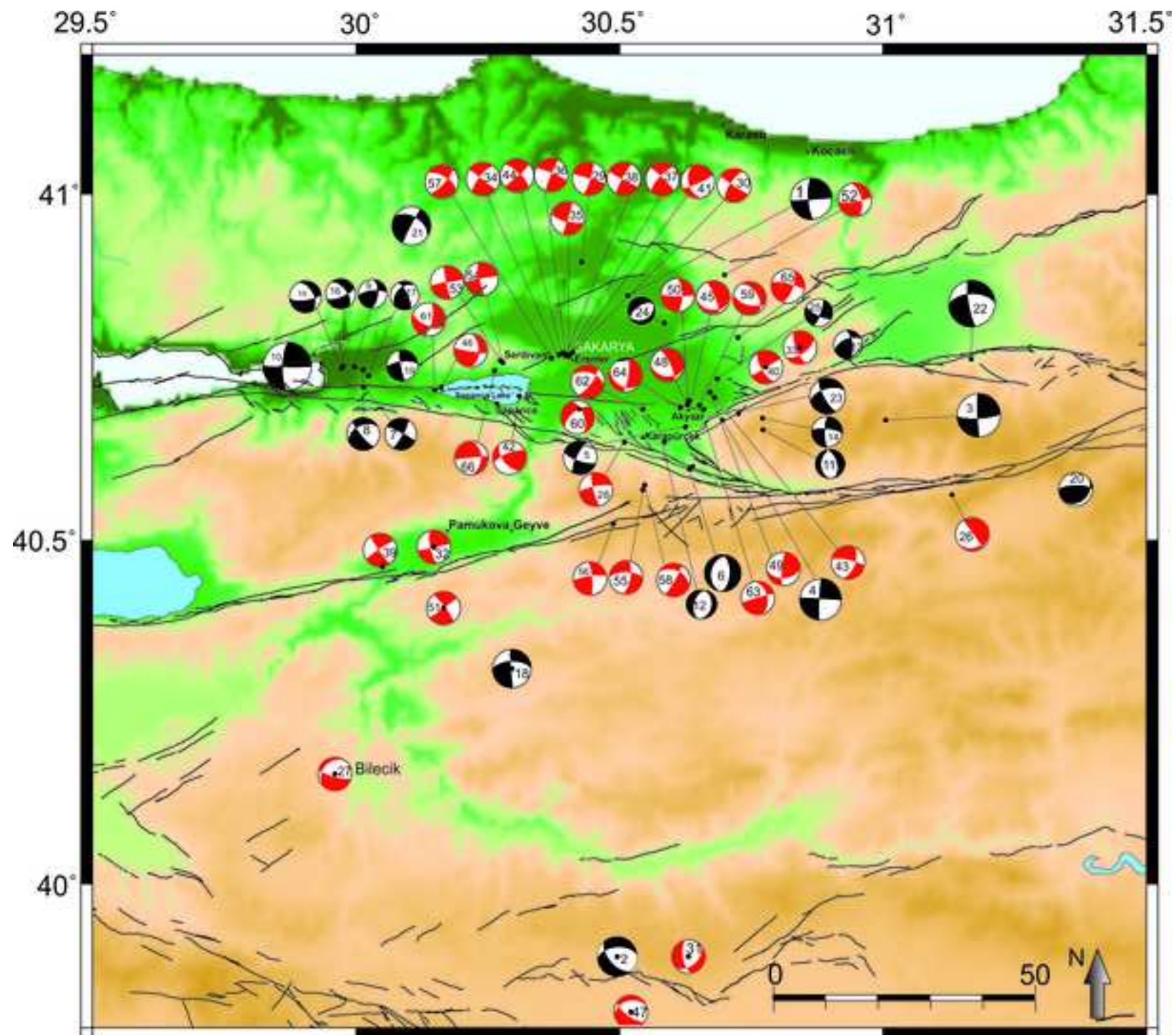
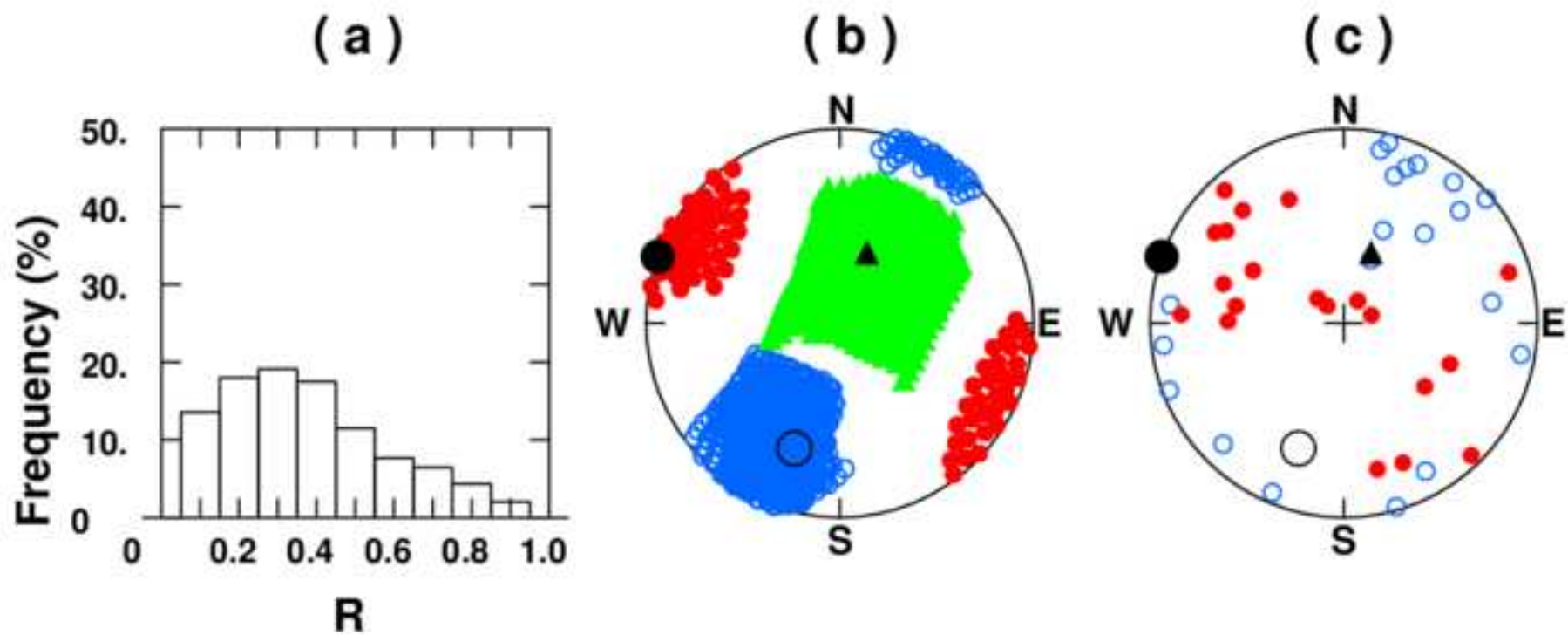


Figure 7
[Click here to download high resolution image](#)



A)



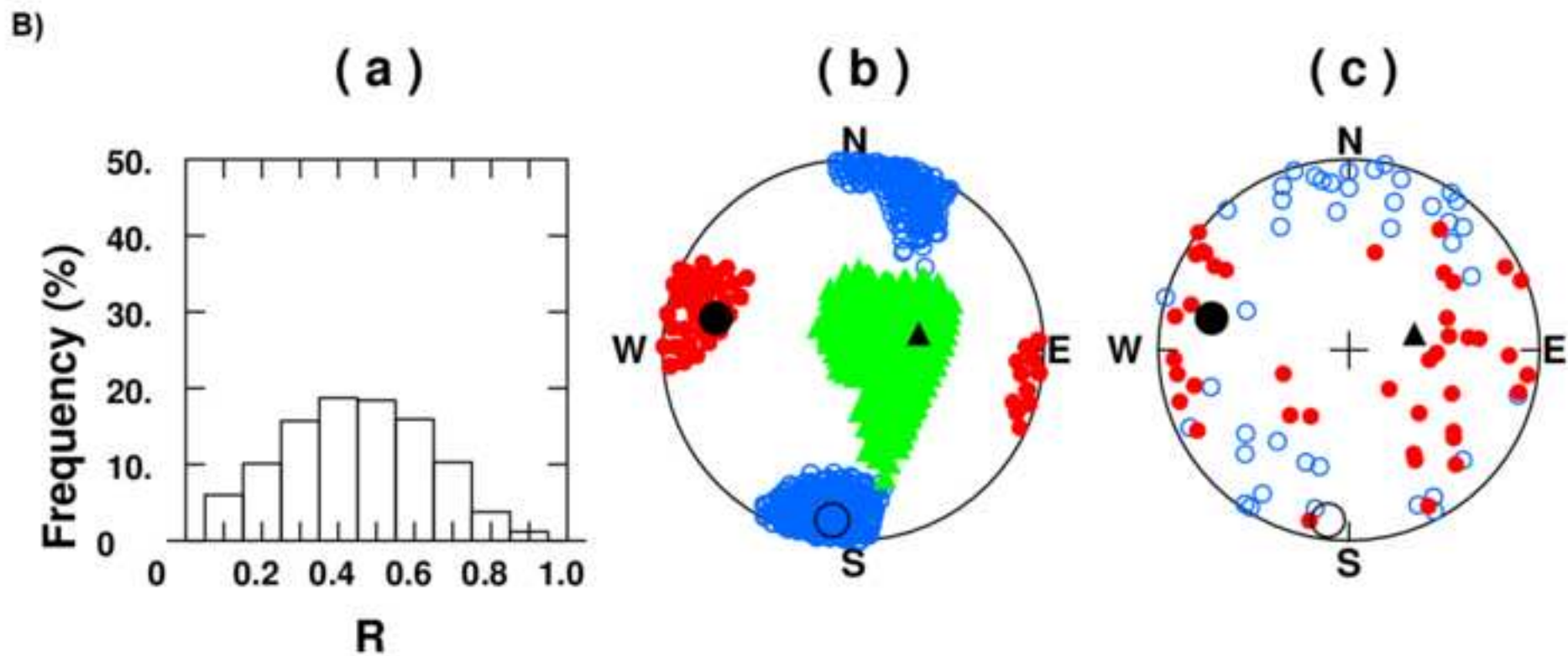


Figure 9a-b
[Click here to download high resolution image](#)

